Journal of Controlled Release 317 (2020) 166–180

Contents lists available at ScienceDirect

Journal of Controlled Release

journal homepage: www.elsevier.com/locate/jconrel

# Catalytic Microgelators for Decoupled Control of Gelation Rate and Rigidity of the Biological Gels

Yu-Tong Hong[a], Daniel T. Bregante[a], Johnny Ching-Wei Lee[a], Yongbeom Seo[a], Dae-Hyun Kim[b], Yong Jae Lee[c], Lawrence B. Schook[d], Hojeong Jeon[e], Hak-Joon Sung[b], David W. Flaherty[a], Simon A. Rogers[a], Hyunjoon Kong[a,f,g,h,*]

[a] Department of Chemical and Biomolecular Engineering, University of Illinois at Urbana-Champaign, Urbana, IL 61801, USA
[b] Department of Medical Engineering, Yonsei University College of Medicine, Seoul 03722, Republic of Korea
[c] Department of Obstetrics and Gynecology, Severance Hospital, Yonsei University College of Medicine, Seoul, 03722, Republic of Korea
[d] Department of Animal Science, University of Illinois at Urbana-Champaign, Urbana, IL 61801, USA
[e] Center for Biomaterials, Biomedical Research Institute, Korea Institute of Science and Technology, Seoul, 02792, South Korea
[f] Department of Bioengineering, University of Illinois at Urbana-Champaign, Urbana, IL 61801, USA
[g] Institute for Genomic Biology, University of Illinois at Urbana-Champaign, Urbana, IL 61801, USA
[h] College of Medicine, University of Illinois at Urbana-Champaign, Urbana, IL, 61801, USA

ARTICLE INFO

*Keywords:*
Fibrin gel
thrombin
$MnO_2$nanosheets
blood clotting
poly(lactic-co-glycolic acid)
hydrogen peroxide

ABSTRACT

Fibrin gels have been extensively used for three-dimensional cell culture, bleeding control, and molecular and cell therapies because the fibrous networks facilitate biomolecular and cell transport. However, a small window for gelation makes it difficult to handle the gels for desired preparation and transport. Several methods developed to control gelation rates often alter the microstructure, thereby affecting the mechanical response. We hypothesized that a particle designed to discharge thrombin cargos in response to an external stimulus, such as $H_2O_2$, would provide control of the gelation rate over a broad range while strengthening the gel. We examined this hypothesis by assembling poly (lactic-co-glycolic acid) (PLGA) particles loaded with thrombin and $MnO_2$ nanosheets that decompose $H_2O_2$ to $O_2$ gas. The resulting particles named as catalytic microgelator were mixed with fibrinogen solution or blood containing 0.2 mM $H_2O_2$. Due to the increased internal pressure, these particles released a 3-fold larger mass of thrombin than PLGA particles loaded only with thrombin. As a consequence, catalytic microgelators increased the gelation time by one order of magnitude and the elastic modulus by a factor of two compared with the fibrin gel formed by directly mixing fibrinogen and thrombin in solution. These catalytic microgelators also served to clot blood, unlike PLGA particles loaded with thrombin. The resulting blood clot was also more rigid than the blood clot formed by thrombin solution. The results of this study would serve as a new paradigm in controlling gelation kinetics of pre-gel solution and mechanical properties of the post-gel matrix.

## 1. Introduction

Fibrinogen in the blood forms a fibrin gel that can control bleeding and further healing of wounds. In general, platelets activated in injuries initiate a coagulation cascade that leads to thrombin formation. Thrombin then converts the water-soluble fibrinogen to the insoluble fibrin by cleaving the fibrinopeptide at the center domain. The resulting active sites react with each other to form a three-dimensional fibrin fiber network. The gel is then further stabilized through chemical crosslinking reaction by factor XIII. [1,2,3,4,5] Fibrin associated with platelets forms blood clots in wounded tissue and acts as a provisional matrix that supports cellular activities essential for wound healing and tissue regeneration [6,7]. Fibrous networks of fibrin gels are advantageous to transporting biomolecules while sequestering cells. Therefore, fibrin gels prepared using isolated or recombinant fibrinogen have also been used for three-dimensional cell cultures, tissue glues, and molecular/cell therapies [8,9,10,11,12].

It is common to assemble fibrin gels by mixing the fibrinogen solution with thrombin molecules in a powder or solution form. [13,14] The quick gelation process leads to difficulties in handling the gel for

*Abbreviations:* PLGA, poly(D,L-lactide-co-glycolide; FRAP, fluorescence recovery after photobleaching

* Corresponding author at: Department of Chemical and Biomolecular Engineering, University of Illinois at Urbana-Champaign, Urbana, IL, 61801, USA.
*E-mail address:* hjkong06@illinois.edu (H. Kong).

https://doi.org/10.1016/j.jconrel.2019.10.029
Received 31 July 2019; Received in revised form 7 October 2019; Accepted 15 October 2019
Available online 11 November 2019
0168-3659/ 

cell encapsulation and implantation [15]. To resolve this challenge, several approaches have been exploited to tune the gelation rate. These approaches include alteration of the concentrations of fibrinogen, thrombin, calcium chloride, and Factor XIII [16,17,18,19]. For instance, decreasing the concentration of thrombin slows the gelation, thus providing users with an increased time window for delivery of the gel. However, the resulting gel presents a significant change in microstructure, where the fiber diameter increases and the branching points decrease. In addition, decreasing thrombin concentration increases the elastic modulus of the fibrin gel. However, a further decrease of the thrombin concentration below 0.25 NIHU/ml softens the gel [2,3].

Overall, it would be desirable to have a tool that provides a broader window for control of gelation while minimally altering the microstructure and mechanical properties of the fibrin gel. We hypothesized that particles discharging thrombin cargos in response to an external stimulus would allow us to decouple the dependency between the gelation time and the mechanics of the fibrin gel. This microparticle, referred to as a catalytic microgelator, would also allow us to avoid altering the concentrations of compounds used for the fibrin gel assembly that affects the microstructure and properties of the fibrin gel.

We examined this hypothesis by using poly(lactic-co-glycolic acid) (PLGA) particles loaded with thrombin and $MnO_2$ nanosheets, denoted as PLGA/$MnO_2$/thrombin particles. Manganese oxide nanosheets catalyze the decomposition of $H_2O_2$ to $H_2O$ and $O_2$ gas. [20,21] Therefore, PLGA/$MnO_2$/thrombin particles suspended in a media containing $H_2O_2$ would increase the internal pressure by generating $O_2$ gas within their interiors. The increased pressure act as an outward force to release thrombin cargos. As a consequence, the increase in thrombin concentration around the particle surface would increase the number of fibrin fibers that sprout from the particle surface (Scheme 1).

In this study, we assessed the extents to which the catalytic microgelator modulates gelation time, microstructure, and mechanical properties of the fibrin gel and blood clot. Catalytic microgelators were mixed with 0.2 mM $H_2O_2$ solution to trigger the thrombin release before mixing them with fibrinogen solution [22,23]. First, we examined the $H_2O_2$ decomposition rate, internal pressure change, and thrombin release rate of catalytic microgelators. In parallel, we monitored the fibrin gel formation by confocal microscopy and small amplitude oscillatory shear (SAOS) measurements. We further characterized the resulting gel by imaging the fibrous structure and measuring the molecular diffusivity and the elastic modulus. To extend our study, we examine the extent to which the catalytic microgelators activate the porcine blood clotting response via SAOS and scanning electron microscopy (SEM). Finally, we employed a rabbit hemorrhage liver model to examine the hemostatic performance of the catalytic microgelators for potential biomedical applications. The results of this study improve the quality of fibrin-based gels used for both fundamental and applied bioscience studies.

## 2. Result and Discussion

### 2.1. Preparation and characterization of PLGA/$MnO_2$ particles encapsulating thrombin (PLGA/$MnO_2$/thrombin particles)

PLGA/$MnO_2$ particles that release thrombin in response to $H_2O_2$ were assembled by encapsulating $MnO_2$ nanosheets and thrombin molecules through the double emulsification. [24,25] Mixing $KMnO_4$ with alginate dissolved in 2-(N-morpholino)ethanesulfonic acid (MES) buffer in 1:1 ratio resulted in the $MnO_2$ nanosheets dispersed in water via reduction of $KMnO_4$ and simultaneous complexation with alginate (Figure S1). [20] The resulting spherical PLGA/$MnO_2$ particles possess a mean diameter of 1.6 ± 0.6 μm, as confirmed with optical microscope images (Fig. 1B and 1C). The incorporation of $MnO_2$ nanosheets in the PLGA particles did not result in a significant change in the diameter of particles and the molecular interaction [26,27] between the particles (Figure S2, S3). The presence of $MnO_2$ nanosheets in the PLGA particle was confirmed by complexing the nanosheets with the rhodamine-conjugated alginate (Fig. 1D). The spherical morphology of the PLGA particle was also confirmed by SEM (Fig. 1E).

The mass of $MnO_2$ nanosheets loaded in 1 mg of particles could be controlled from 0.0625 to 6.25 μg by altering the initial concentration of $MnO_2$ nanosheets added to the aqueous media during the double emulsification. The loading mass of thrombin was minimally affected by the loading mass $MnO_2$ nanosheets in the particles. According to the thrombin ELISA kit, 1 mg of PLGA and PLGA/$MnO_2$ particles carried 72 ± 1.6 ng of thrombin. The small loading error range influenced the drug release profile insignificantly. We also evaluated the potential toxicity of the PLGA and PLGA/$MnO_2$ particles by measuring the

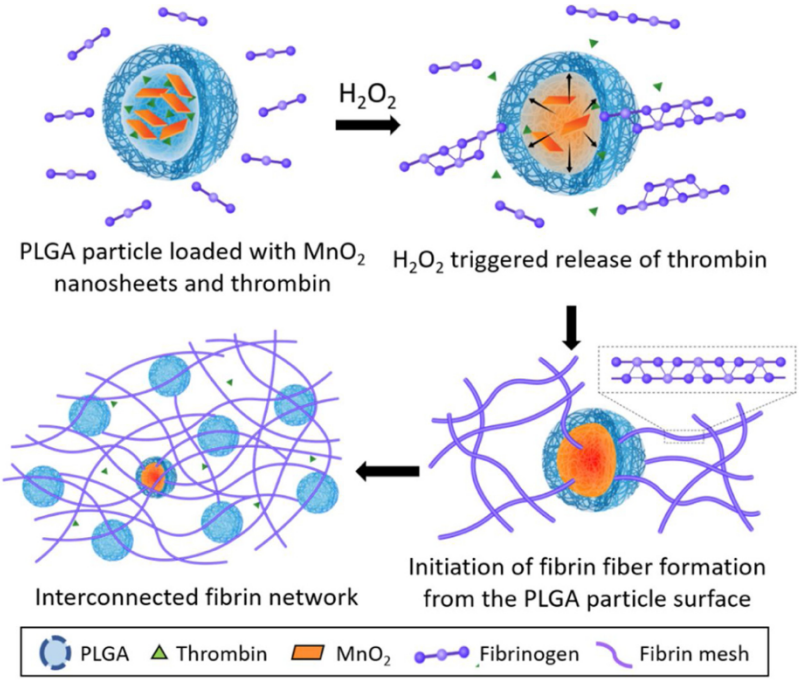


**Scheme 1.** Schematic illustration of the process to form fibrin networks in which fibrin fibers are interconnected with PLGA/$MnO_2$/thrombin particles (i.e., PLGA particles loaded with catalytic $MnO_2$ nanosheets and thrombin). $H_2O_2$ triggers continuous release of thrombin cargos from PLGA/$MnO_2$/thrombin particles and, in turn, increase the internal pressure of particles. The released thrombin initiates polymerization of fibrinogen on the PLGA particle surface and promotes the sprouting of fibrin fibers.

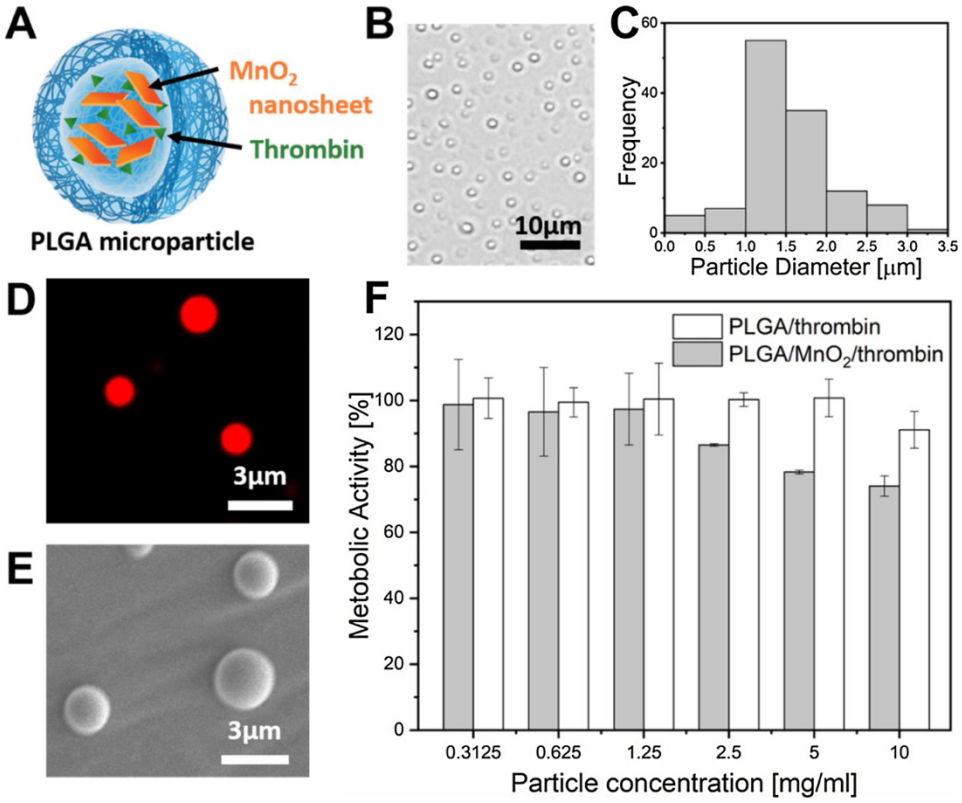


**Fig. 1.** Characterization of PLGA/$MnO_2$/thrombin microparticles. (A) Schematic illustration of PLGA/$MnO_2$/thrombin particles. (B) Optical microscopic image of PLGA/$MnO_2$/thrombin particles. (C) The size distribution of microparticles analyzed with optical microscope images. (D) Confocal image of PLGA/$MnO_2$/thrombin microparticles. $MnO_2$ nanosheets were labeled with red-colored rhodamine. (E) SEM image of PLGA/$MnO_2$/thrombin particles. (F) Quantification of the metabolic activity of C166 endothelial cells after incubation with PLGA or PLGA/$MnO_2$ particles over 24 hours. PLGA/$MnO_2$ particles used herein are assembled by loading 6.25 μg of $MnO_2$ nanosheets in 1 mg of particles. In (F), data points and error bars represent the average values and standard deviation of three samples, respectively.

metabolic activity of endothelial cells incubated with these particles for 24 hrs. Up to the particle concentration of 10 mg/mL, more than 70 % of cells remained metabolically active (Fig. 1F).

### 2.2. Kinetic study of $H_2O_2$ decomposition by PLGA/$MnO_2$ particles

We examined the extent to which PLGA/$MnO_2$ particles take up and decompose $H_2O_2$ by measuring peroxide-induced oxidation of ferrous to ferric ions. Both fresh and lyophilized PLGA/$MnO_2$ particles decreased $H_2O_2$ concentration from 0.2 to 0.15 mM continuously over 7 hours (Fig. 2A). In contrast, the direct addition of $MnO_2$ nanosheets to the $H_2O_2$ solution resulted in rapid decomposition, as reported before. [20,28,29] The $H_2O_2$ concentration decreased from 0.2 Mm to almost 0 mM within an hour. In addition, blank PLGA microparticles did not decompose $H_2O_2$.

We calculated the amount of $O_2$ generated within the particle by using the stoichiometric relationship between decomposed $H_2O_2$ and generated $O_2$ (Figure S4). According to the calculation, both fresh and lyophilized PLGA/$MnO_2$ particles produced $O_2$ gas continuously up to 7 hours. The lyophilized PLGA/$MnO_2$ particles generated $O_2$ gas more actively than fresh ones, likely due to the more rapid diffusion of $H_2O_2$ into the particle.

We further examined the kinetics of $H_2O_2$ decomposition by monitoring visible absorbance at 454 nm, after titration with a $Cu^{II}$ and neocuproine (Fig. 2B) [30]. The initial $H_2O_2$ decomposition rate was quantified with a slope of the linear portion of each curve shown in Fig. 2B. The $H_2O_2$ decomposition rate by lyophilized PLGA/$MnO_2$ particles was twice as high as that observed by fresh PLGA/$MnO_2$ particles (Fig. 2C). This result also suggests that $H_2O_2$ diffuses into lyophilized PLGA/$MnO_2$ particles more rapidly than fresh particles due to pore formation in the particle shell after lyophilization. [31,32] The decomposition rate by blank PLGA particles was zero.

In addition, we evaluated the degree that $H_2O_2$ decomposition rate depends on the $H_2O_2$ concentration during reactions on $MnO_2$ nanosheets (Fig. 2D and Figure S5). In this study, we compared the decomposition activity of lyophilized PLGA/$MnO_2$ particles with that of free $MnO_2$ nanosheets. The decomposition rate exhibited a nearly linear dependence on $H_2O_2$ concentration for both free $MnO_2$ nanosheets (rate $\sim [H_2O_2]^{0.9 \pm 0.04}$) and lyophilized PLGA/$MnO_2$ particles (rate $\sim [H_2O_2]^{0.9 \pm 0.05}$).

The activation energy for $H_2O_2$ decomposition ($E_a$) was calculated by fitting the curve of the decomposition rate constant ($k$; calculated by assuming a pseudo-first-order rate expression on $H_2O_2$ concentration) versus inverse temperature to the Arrhenius equation.

$$k = \nu e^{\left(\frac{-E_a}{RT}\right)} \quad (1)$$

Where $\nu$ is the pre-exponential factor, $R$ is the ideal gas constant, and $T$ is the absolute temperature (Fig. 2E and Figure S6). The activation energy with free $MnO_2$ nanosheets (44 ± 4 kJ/mol) is comparable to $E_a$ attained with lyophilized PLGA/$MnO_2$ particles (49 ± 5 kJ/mol). The similarity of the $H_2O_2$ decomposition rates, power-law dependencies, and activation energies suggest that the integration of $MnO_2$ nanosheets into PLGA particles does not significantly affect the rate or the mechanism for $H_2O_2$ decomposition on these materials.

The lyophilized PLGA/$MnO_2$ particles were able to protect cells from $H_2O_2$ (Fig. 2F). We exposed endothelial cells to the $H_2O_2$ or the mixture of $H_2O_2$ and PLGA/$MnO_2$ particles for 24 hours and examined the metabolic activity of cells. 90 % of cells lost metabolic activity in the media containing 0.3 and 0.6 mM $H_2O_2$. In contrast, approximately 90 % of cells incubated with PLGA/$MnO_2$ particles remained metabolically active up to 0.6 mM $H_2O_2$ solutions. This protective effect is due to the uptake and decomposition of $H_2O_2$ by the $MnO_2$ within the PLGA/$MnO_2$ particles.

### 2.3. Analysis of thrombin release from particles

The ability of thrombin-encapsulating PLGA and PLGA/$MnO_2$ particles to release thrombin cargos was evaluated by measuring the mass of thrombin discharged from the particles (Fig. 3A). The particles were incubated in neutral PBS with 0.2 mM $H_2O_2$. The 0.2 mM concentration

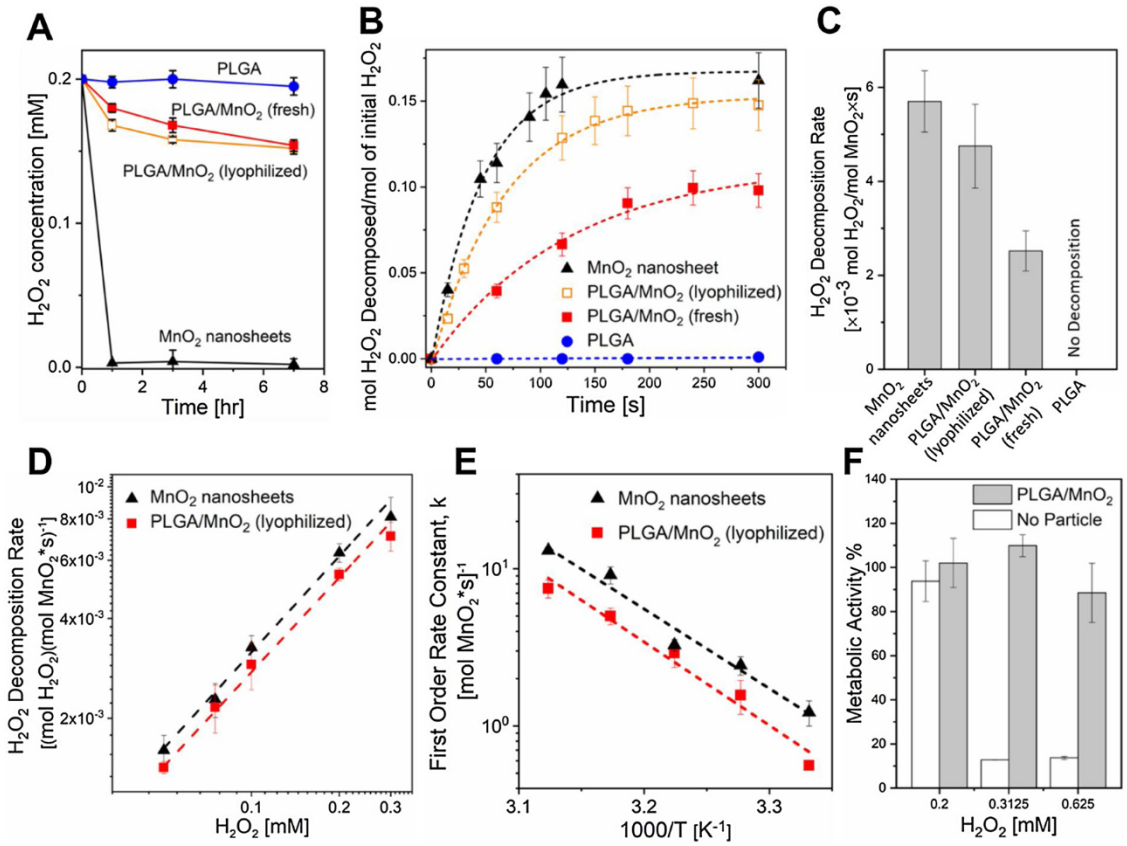


**Fig. 2.** Kinetic and thermodynamic analysis of the $H_2O_2$ decomposition activated by PLGA/$MnO_2$ particles, PLGA particles, and free $MnO_2$ nanosheets. (A) Measurement of the $H_2O_2$ concentration change over time. Particle concentration in the $H_2O_2$ solution was kept constant at 5 mg/ml. (B) The mole of $H_2O_2$ decomposed per mole of initial $H_2O_2$ during the first 5 min. Particle concentration in the $H_2O_2$ solution was kept constant at 1 mg/ml. Dashed lines are for visual guide. (C) Initial $H_2O_2$ decomposition rate quantified by fitting curves in (B). (D) The dependency of the decomposition rate on the $H_2O_2$ concentration for free $MnO_2$ nanosheets (▲) and lyophilized PLGA/$MnO_2$ particles (■). (E) Dependence of the decomposition rate on temperature for free $MnO_2$ nanosheets (▲) and lyophilized PLGA/$MnO_2$ particles (■). (F) Metabolic activity of C166 endothelial cells after incubation with PLGA/$MnO_2$ particles in 0.2-0.625 mM $H_2O_2$ solution. In (A)–(F), each data point and error bar represent the average and standard deviation of three different samples per condition, respectively. In this study, the mass of $MnO_2$ in the 1 mg of PLGA/$MnO_2$ particles was kept constant at 6.25 μg.

was chosen because it is sufficient to trigger the active release of thrombin without damaging particles, according to our previous study. [20] The $H_2O_2$ level also falls in the range of the physiological concentration of $H_2O_2$ [22,23,33]. Thrombin molecules burst out within the first hour. Thrombin molecules partially embedded in the surface layer of the particles contribute mainly to this initial burst [34,35]. During 7 hours, fresh PLGA/$MnO_2$ particles, in which 6.25 μg of $MnO_2$ nanosheets were loaded into 1 mg of particles, released three times more thrombin than PLGA particles. Lyophilized PLGA/$MnO_2$ particles released thrombin faster than fresh particles. In contrast, PLGA/$MnO_2$ particles, in which 62 ng of $MnO_2$ nanosheets were loaded in 1 mg of particles, released thrombin cargos with a similar profile to PLGA particles. Thus, PLGA/$MnO_2$ particles (1 mg) encapsulated with 6.25 μg $MnO_2$ nanosheets were used in the rest of the study.

The $H_2O_2$-responsive release of thrombin is attributed to the generation of oxygen that increases the internal pressure of particles. [20] The total flux of thrombin across PLGA particles ($J_s$) after the initial burst (1-20 hour) was correlated to the pressure difference between inside and outside particles ($\Delta P$). The $\Delta P$ value of particle was calculated for each group using the ideal gas law for $O_2$ gas. The mass of $O_2$ shown in Figure S2 was used in the calculation. (Calculation of $\Delta P$ is detailed in the Supporting Information). The calculated $\Delta P$ values for lyophilized and fresh PLGA/$MnO_2$ were 10.3 mmHg and 9.8 mmHg, respectively. In contrast, PLGA particles free of $MnO_2$ only exhibited a minimal pressure difference of 2.1 mmHg (Table S1). As shown in Fig. 3B, the release rate ($J_s$) of thrombin molecules was linearly related to the calculated ΔP.

The linear dependence of $J_s$ on $\Delta P$ confirms that enhanced release of thrombin cargos from PLGA/MnO2/thrombin particles is primarily due to the $\Delta P$, which is well-described by the Kedem-Katchalsky equation. [36,37] The equation relates $J_s$ to the flux driven by the hydraulic pressure difference and that induced by the diffusion as shown in Eq. (2).

$$J_s = a\Delta c + b\Delta P \quad (2)$$

Where $a = RT[\omega - \sigma(1-\sigma)\bar{c}L_p]$ and $b = (1-\sigma)\bar{c}L_p$ are constant values, $\Delta c$ is the concentration difference of thrombin between particle interior and exterior, and $\Delta P$ is the hydraulic pressure difference between inside and outside of the particle. $R$ represents the gas constant, $T$ the temperature, and $\bar{c}$ is the average concentration of thrombin across the particle. $L_p$, ⌉, and ⌈ are transport coefficients of filtration, solute permeability, and reflection coefficients of PLGA particle, respectively. In Eq. (2), $\Delta c$ was approximated as a constant, equal to the concentration of thrombin inside the particle because the concentration of thrombin within the particle was several orders of magnitude higher than that outside the particle. Thus, $J_s$ becomes primarily dependent on $\Delta P$ [20].

To confirm the $O_2$-induced release of particles, we examined the spatial distribution of fluorescently-labeled $MnO_2$ nanosheets in the PLGA/$MnO_2$ particles upon exposure to $H_2O_2$ using confocal microscopy (Fig. 3C). $MnO_2$ nanosheets were distributed uniformly within the particle suspended in PBS. In contrast, the particles incubated in the PBS supplemented with 0.2 mM $H_2O_2$ displayed the localization of

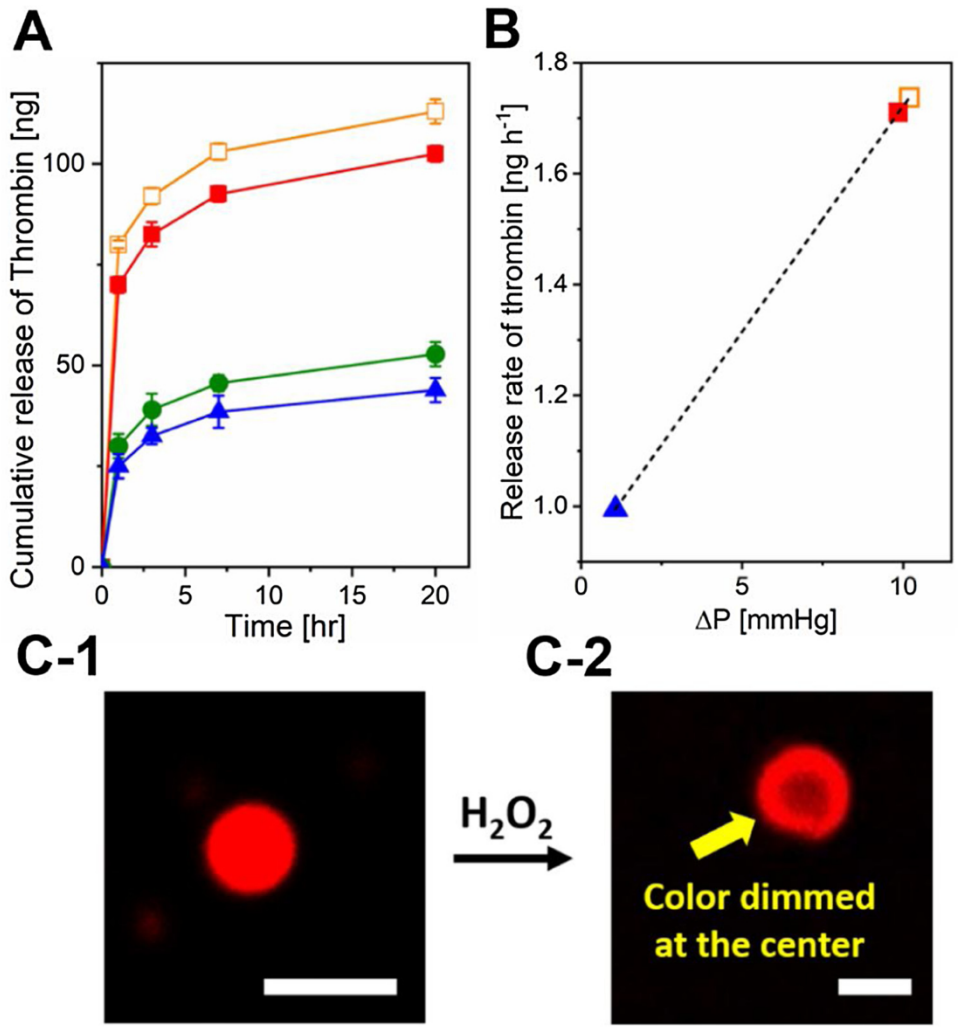


**Fig. 3.** Analysis of the $H_2O_2$-triggered thrombin release profile and underlying mechanism (A) Cumulative release profile of thrombin from the PLGA/$MnO_2$/thrombin particles with a loading of $MnO_2$ at 6.25 μg/mg particle (-■-: fresh particle and -□-: lyophilized particle) and at 0.0625 μg/mg particle (-●-); -▲-: Cumulative release profile of thrombin from PLGA particles. The particles were incubated in PBS dissolved with $H_2O_2$ (0.2 mM $H_2O_2$). (B) The release rate of thrombin versus the hydraulic pressure difference (ΔP) between inside and outside of the lyophilized PLGA/$MnO_2$/thrombin particles (-□-), fresh PLGA/$MnO_2$/thrombin particles (-■-), and PLGA/thrombin particles (-▲-). In (A), data points and error bars represent the average and standard deviation of three different samples per condition, respectively. (C) Confocal image of PLGA/$MnO_2$ particles loaded with rhodamine-labeled $MnO_2$ nanosheets. In PBS, $MnO_2$ nanosheets were distributed uniformly in the particle (C-1). In contrast, particles incubated in 0.2 mM $H_2O_2$ solution showed the localization of rhodamine-labeled $MnO_2$ nanosheets to the particle wall, due to $O_2$-induced pressurization (C-2). Scale bars represent 3 μm. The mass of $MnO_2$ in the 1 mg of PLGA/$MnO_2$ particles was kept constant at 6.25 μg.

$MnO_2$ nanosheets to the particle wall. This result indicates that PLGA/$MnO_2$ particles increase the internal pressure due to the oxygen generation. Most of the $MnO_2$ nanosheets remained in the particles during $H_2O_2$-triggered thrombin release, as confirmed by the lack of change in the red fluorescence over time (Figure S7).

### 2.4. Microstructural Analysis of Fibrin Gel Formation

We examined the extent to which the $H_2O_2$-mediated thrombin release rate modulates the fibrin gel formation by visualizing the fibrous network formation process (Fig. 4A and B). We encapsulated 72 ng of thrombin into 1 mg of PLGA or PLGA/$MnO_2$ particles. The loading amount of $MnO_2$ nanosheets was kept constant at 6.25 μg per mg of particles. The particles were mixed with an aqueous mixture of fluorescently-labeled fibrinogen and $H_2O_2$. The concentration of $H_2O_2$ in the fibrinogen solution was kept constant at 0.2 mM.

According to the real-time confocal images, thrombin-encapsulating PLGA/$MnO_2$ particles (PLGA/$MnO_2$/thrombin particles) served to form fibrin networks more rapidly than thrombin-encapsulating PLGA particles (PLGA/thrombin particles) (Fig. 4B). The quantitative image analysis conducted by counting the fibrin fibers disclosed that PLGA/$MnO_2$/thrombin particles increased the total number of fibrin fibers by a factor of two (Fig. 4C). PLGA/$MnO_2$/thrombin particles associated with the fibrin network, while PLGA/thrombin particles clustered together (Figure 4D-1 and D-2). The aggregation of PLGA/thrombin particles in the fibrin gel likely results from the hydrophobic interaction between the particles that do not associate with fibrin fibers. [38]

According to the SEM images of the gel, PLGA/MnO2/thrombin particles resulted in the fibrin gel with similar microstructure to the gel made using the thrombin solution, as evaluated with the fiber diameter and the number and density of branching points (Fig. 5). In addition, PLGA/$MnO_2$/thrombin particles were connected with multiple fibrin fibers (Fig. 5E). In contrast, the fibrin gel formed by PLGA/thrombin particles (Fig. 5C and 5 F) showed a thicker fibrin fiber and a smaller number of branching points than two other conditions. (Fig. 5F).

We propose that PLGA/$MnO_2$/thrombin particles release thrombin rapidly to increase the fibrinogen cleavage rate, compared with PLGA/thrombin particles. The resulting fibrinogen monomers serve to increase the number of branching points of fibrin networks instead of promoting longitudinal and lateral growth [3]. In addition, the anchorage of fibrin fibers to PLGA/$MnO_2$/thrombin particles suggests that thrombin released from the particles activate the polymerization of fibrinogen on the particle surface and promote the sprouting of fibrin fibers (Fig. 5E). In contrast, PLGA/thrombin particles cleave fibrinopeptide at a lower rate than PLGA/$MnO_2$/thrombin particles due to the slow release of thrombin. As a consequence, fibrinogen monomers tend to polymerize into long fibers and then associate laterally to form thick fibers, as shown in Fig. 5F.

Permeability of the gel was examined by measuring a diffusion coefficient of dextran within the gel (Fig. 6A and 6B) [39,40]. Dextran probes labeled with fluorescein were loaded into the fibrin gel for the FRAP assay. The diffusion coefficient of dextran was calculated from the fluorescence recovery rate in the photobleached spot (details are in the experimental section). The fibrin gel prepared with PLGA/$MnO_2$/

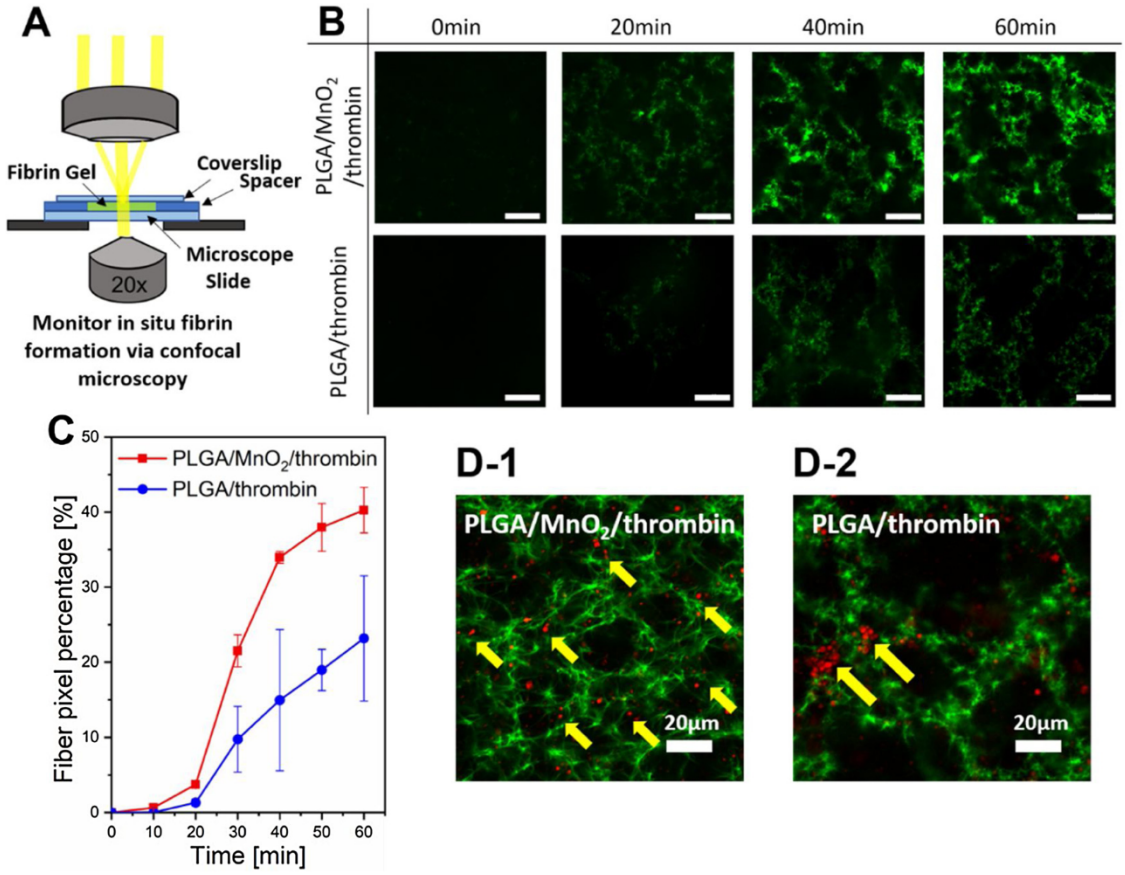


**Fig. 4.** Image analysis of fibrin network formation modulated by PLGA/$MnO_2$/thrombin or PLGA/thrombin particles. (A) Schematic illustration of the experimental set-up to monitor fibrin formation in situ using confocal microscopy. (B) Confocal microscopy images of the fibrin fiber network formation over time. Fibrin was labeled with fluorescein. The fibrin gel was formed by mixing fibrinogen solution, 0.2 mM $H_2O_2$ solution, and PLGA/$MnO_2$/thrombin or PLGA/thrombin particles. The concentration of the $H_2O_2$ solution in the final mixture was kept constant at 0.2 mM. Scale bars represent 30 μm. (C) Quantification of the fibrin fiber pixel increased over time. Data points and error bars represent the average value and the standard deviation of three different samples per condition, respectively. (D) Confocal microscopy image of the fibrin networks (green color) and particles used to release thrombin (red color). (D-1) Fibrin networks formed using the PLGA/$MnO_2$/thrombin particles. (D-2) Fibrin networks formed using the PLGA/thrombin particles. In this study, the mass of $MnO_2$ and thrombin in the 1 mg of PLGA/$MnO_2$/thrombin particles were kept constant at 6.25 μg and 72 ng, respectively. The mass of thrombin in the 1 mg of PLGA/thrombin particles was kept constant at 72 ng. The mass ratio between fibrinogen and particles was kept constant at 1:4.

thrombin particles decreased the diffusion coefficient of the dextran by a factor of two compared with PLGA/thrombin particles (Fig. 6C).

We further evaluated the bio-adhesion of the fibrin gel to tissue by filling the wound-mimicking hole introduced in a porcine skin explant with the gel (Figure S8). Then, we observed infiltration of fibrin networks to the skin tissue using SEM. The gels prepared using the PLGA/$MnO_2$/thrombin particle and PLGA/thrombin particles anchored to the skin explant similar to the gel prepared with a mixture of fibrinogen and thrombin. We also characterized the surface hydrophilicity of the gels by measuring the water contact angle [41,42]. The thrombin released from PLGA particles did not alter the water contact angle on the fibrin gel surface significantly compared with the thrombin solution mixed with fibrinogen solution (Figure S9).

### 2.5. Rheological Characterization of Fibrin Gel Formation

One major advantage of using PLGA/MnO2/thrombin particle-based gelator in the preparation of fibrin gels is to broaden the time window for gel preparation without reducing gel rigidity. This process is different from the conventional preparation method of the fibrin gel in which fibrinogen solution is mixed with the thrombin solution or powders. Branching points of the fibrin gel are responsible for the elastic response of the gel [2]. We, therefore, monitored the gelation process by measuring the storage modulus of the gel over time (Fig. 7A). Notably, mixing fibrinogen with the thrombin solution increased the storage modulus to 180 Pa within 5 minutes, with no significant increase after 5 minutes (Figure 7B-1). Mixing fibrinogen, thrombin, and blank PLGA particles exhibited a limited increase in the storage modulus to 3 Pa. This result implies that blank PLGA particles that are not releasing thrombin molecules do not participate in forming the gel network. Instead, blank PLGA particles act as a physical barrier of the fibrin gel formation.

In the presence of $H_2O_2$, catalytic PLGA/$MnO_2$/thrombin particles served to increase the storage modulus of the gel continuously over 100 minutes. The storage modulus eventually reached approximately 250 Pa after 2.5 hours. In contrast, non-catalytic PLGA/thrombin particles led to a softer network than PLGA/$MnO_2$ particles, as indicated by the lower storage modulus throughout the measurements (Figure 7B-2). The storage modulus at 3.75 hours after initiation of gelation was quantified as the equilibrium storage modulus, denoted as $G'_{eq}$, because no significant increase occurred beyond this time. The equilibrium storage modulus of the gel formed by mixing thrombin solution with fibrinogen was defined as the storage modulus at 25 minutes after initiation of gelation. $G'_{eq}$ of the gel prepared by the PLGA/$MnO_2$/thrombin particles was 33% higher than the fibrin gel prepared by mixing fibrinogen and thrombin solution, 71% higher than that of the fibrin gel prepared with the PLGA/thrombin particles, and 350% higher than that of the fibrin gel prepared by mixing fibrinogen, thrombin, and

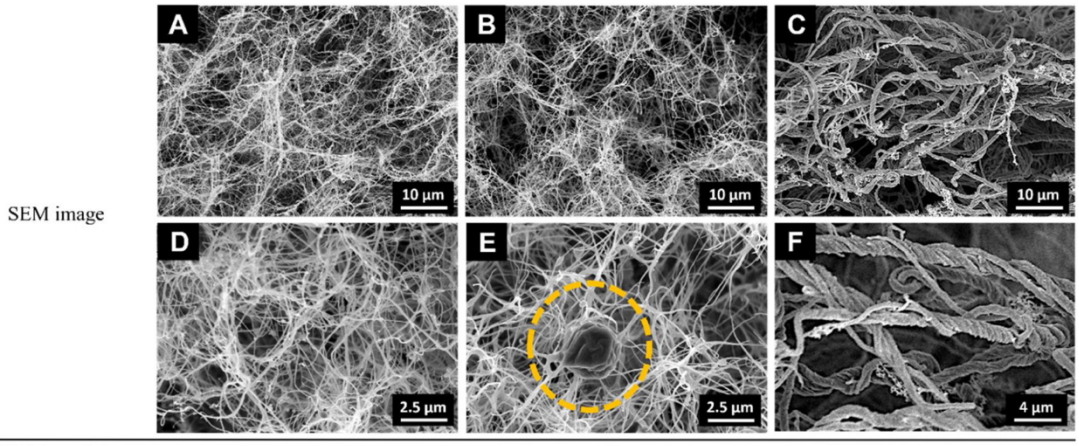


| | | | |
|---|---|---|---|
| PLGA particle | - | + | + |
| Thrombin in solution | + | - | - |
| Thrombin in particle | - | + | + |
| $MnO_2$ | - | + | - |
| Fiber Diameter | $0.15 \pm 0.05\ \mu m$ | $0.14 \pm 0.04\ \mu m$ | $0.92 \pm 0.27\ \mu m$ |
| # of Branch points | 2140 | 1829 | 894 |
| Branch point Density | $0.768\ \mu m^{-2}$ | $0.741\ \mu m^{-2}$ | $0.321\ \mu m^{-2}$ |

**Fig. 5.** Analysis of the microstructure of the fibrin gel captured using SEM. (A & D) The fibrin gel formed by mixing fibrinogen (2.5 mg/mL) and thrombin (0.25 IU/mL). (B & E) The fibrin gel formed by mixing PLGA/$MnO_2$/thrombin particles (10 mg/mL), fibrinogen solution (2.5 mg/mL), and $H_2O_2$ (0.2 mM). 6.25 μg of $MnO_2$ nanosheets were loaded in the 1 mg of PLGA/$MnO_2$ particles. (C & F) The fibrin gel formed by mixing PLGA/thrombin particles (10 mg/mL), fibrinogen solution (2.5 mg/mL), and $H_2O_2$ (0.2 mM). The fiber diameter, number of branching points, and branching point density were noted in the table under corresponding images. In this study, the mass of thrombin in the 1 mg of particles was kept constant at 72 ng.

blank PLGA (Figure 7C). We propose that the difference between these conditions is attributed to the short half-life of thrombin. In particular, the PLGA/$MnO_2$/thrombin particles serve to release biologically active thrombin and create reactive sites of fibrinogen to polymerize continuously, while the thrombin dissolved in solution loses bioactivity quickly [43]. Furthermore, due to the connection of particles with interconnected fibrin fibers, the equilibrium storage moduli of the gel formed by thrombin releasing particles (e.g., PLGA/$MnO_2$/thrombin particles and PLGA/thrombin particles) are significantly higher than the storage modulus of the fibrin gel made with a mixture of fibrinogen, thrombin and blank PLGA particles.

In parallel, the time required to reach a stiffness equal to one half of $G_{eq}^{'}$, denoted $t_{1/2}$, was quantified to assess the time window required for gel fabrication (Fig. 7D). While the $t_{1/2}$ of PLGA/$MnO_2$/thrombin particles was five times larger than the mixture of fibrinogen and thrombin, $t_{1/2}$ was significantly smaller than that attained with the PLGA/thrombin particles. The difference in $t_{1/2}$ between PLGA/$MnO_2$/thrombin and PLGA/thrombin particles is in accordance with the thrombin release and kinetic study, where the faster release of thrombin leads to smaller $t_{1/2}$. $t_{1/2}$ for the mixture of fibrinogen, thrombin, and PLGA particles was comparable to that with the PLGA/thrombin particles. This result indicates that the fibrin gelation process can be modulated by tuning the thrombin release profile from the particles. The accelerated release of thrombin from the PLGA/$MnO_2$/thrombin particles led to a decrease in the gelation time [3]. We propose that a further increase in particle concentration will facilitate the gelation process due to the increase in total mass of thrombin in the pre-gelled fibrinogen solution. However, excess particles can act as physical barriers for the growth of fibrin fibers, which is implicated in Fig. 7C. More in-depth relationship between particle concentration and gel stiffness will be of interest for future study.

We further fitted the storage modulus-time curves in Fig. 7B to a simple model proposed for a blood coagulation process (Eq. (3)) [44],

$$G^{'}(t) = G'_{eq}\exp(-\beta/t) \quad (3)$$

in which $G_{eq}^{'}$ represents the equilibrium storage modulus, $\beta$ is the characteristic time, and $t$ indicates the time scale of gelation (Figure S10). This single exponential model gave a good fitting quality ($R^2 = 0.994$) for the gelation process (Table 1). PLGA/$MnO_2$/thrombin particles resulted in the five-fold increase in $\beta$ compared with the mixture of fibrinogen and thrombin solutions where the smaller $\beta$ represents faster gelation. The PLGA/$MnO_2$/thrombin particles led to the smaller $\beta$ than PLGA/thrombin particles. However, the relatively low $R^2$ value with PLGA/$MnO_2$/thrombin particles (i.e., 0.93) indicates that the single exponential model may not sufficiently describe the gelation caused by the microparticles.

Therefore, the evolution of the storage modulus was decomposed into two reaction phases, as proposed by Kaibara. [45] The first phase corresponds to the elastic response caused mainly by the polymerization and branching of fibrin fibers, while the other represents the elastic response associated with the lateral association of fibrin polymers. As shown in Fig. 7, the storage modulus increases more steeply during the first phase. To separate the distinct contributions, we exploited the double exponential model [45] (Eq. (4)),

$$G^{'}(t) = G'_0 + G^{'}_1\left(1 - \exp\left(-\frac{t}{\tau_1}\right)\right) + G^{'}_2\left(1 - \exp\left(-\frac{t}{\tau_2}\right)\right) \quad (4)$$

in which $G_0^{'}$ is the storage modulus of the pre-gelled solutions, $G_1^{'}$ is the storage modulus contributed by the first branching and crosslinking reaction phase, $G_2^{'}$ is the storage modulus caused by the second lateral growth of fibrin polymers, and $1/\tau_1$ and $1/\tau_2$ are the characteristic rates for branching and lateral growth, respectively (Fig. S11).

As shown in Table 2, PLGA/$MnO_2$/thrombin particles showed slower rates of branching ($1/\tau_1$) and lateral growth ($1/\tau_2$) than the mixture of fibrinogen and thrombin by one and two orders of magnitude, respectively. Combined with the higher $G_1^{'}$ and $G_2^{'}$ values, this result confirms the advantages of using PLGA/$MnO_2$/thrombin particles to form a stiffer network while expanding the time window for gelation. In addition, PLGA/$MnO_2$/thrombin particles led to a faster branching rate ($1/\tau_1$) than PLGA/thrombin particles due to the faster release of

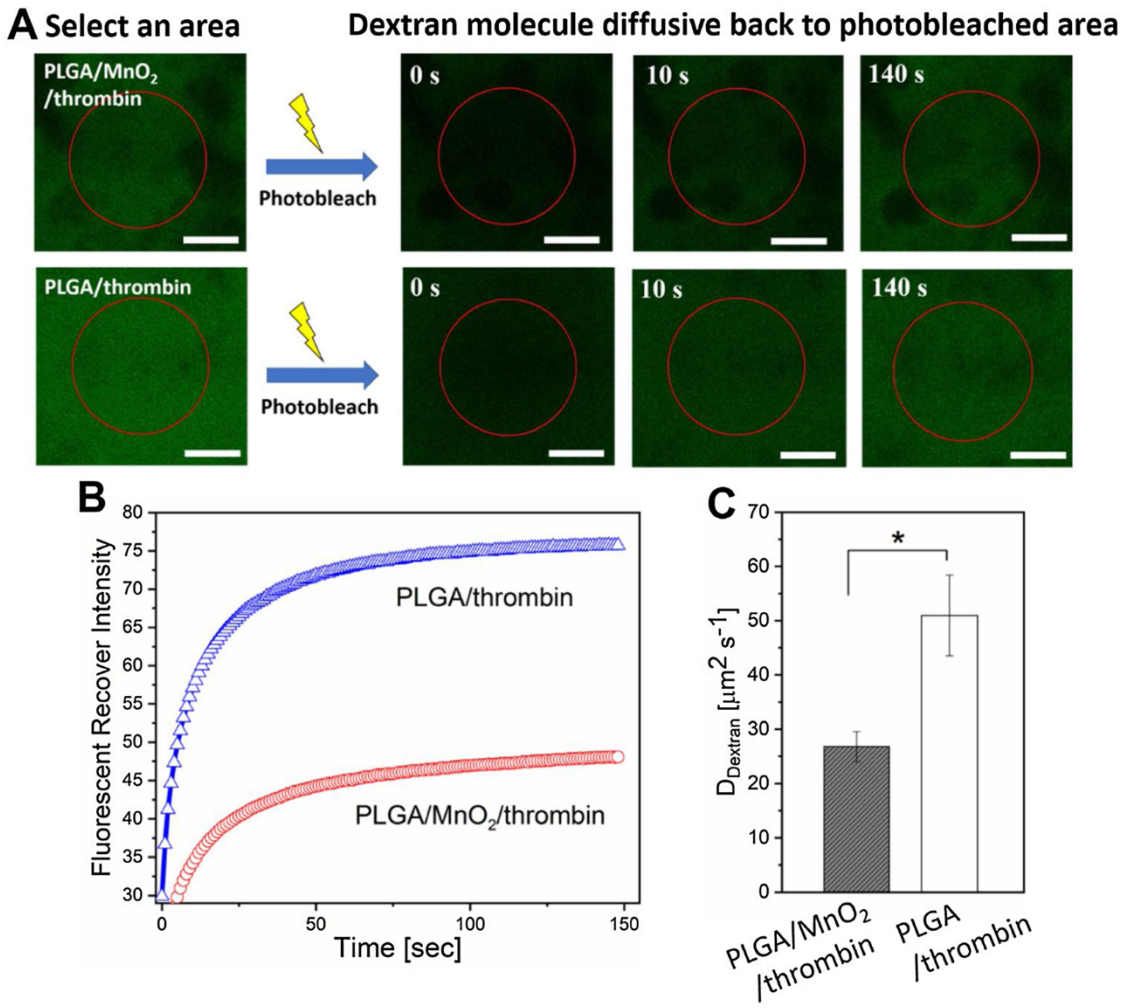


**Fig. 6.** FRAP analysis of dextran probes in fibrin gels made using PLGA/$MnO_2$/thrombin or PLGA/thrombin particles. (A) Confocal microscopy image of the fibrin gel that undergoes fluorescence recovery after photobleaching. The images were used to quantify the diffusion coefficient of the fluorescently labeled dextran (green color, $D_{dextran}$). The scale bar represents 10 μm. (B) Quantified fluorescent intensity of the dextran molecule in the photobleached area over time. (C) Quantification of $D_{dextran}$ in the fibrin gel. Data points and error bars represent the average and standard deviation of three different samples per condition, respectively. The composition of the particles used in this study was same as the condition in Fig. 4. * represents the statistical significance of the difference in the values between the two indicated groups (*$p < 0.05$).

thrombin molecules. The rate of lateral growth ($1/\tau_2$) had no significant difference. This result suggests that thrombin released from PLGA/$MnO_2$ particles mainly contributes to increasing the number of branching points of fibrin networks.

We further examined whether the fibrin gel formed using the PLGA/$MnO_2$/thrombin particles modulate activities of endothelial cells to form blood vessel-like lumens similar to the gel formed using the thrombin solution [46]. In this study, we loaded human umbilical vein endothelial cells (HUVECs) within fibrin gels of interests installed in the center channel ② of a microfluidic chip assembled for neovascularization study (Figure. S12). As the vascular endothelial growth factors (VEGF) diffuse from the outer channels ① and ③ to the HUVEC-laden fibrin gel, cells assembled to form interconnected endothelial lumens. Likely due to the similar fibrous structure between two fibrin gel systems, the length and the number of resulting endothelial lumens were similar to each other.

### 2.6. Rheological Characterization of Blood Clotting Promoted by PLGA/$MnO_2$/thrombin Particles

We further evaluated the efficacy of PLGA/$MnO_2$/thrombin microparticles to activate the blood clotting in response to $H_2O_2$. In this study, 3.2% buffered sodium citrate was added to porcine blood to prevent instantaneous clotting after blood collection. The PLGA/$MnO_2$/thrombin particles were mixed with $H_2O_2$ solution (0.2 mM) to activate the release of thrombin cargos. Then, the particles were added to the blood. The blood mixed with the PLGA/$MnO_2$/thrombin particles formed a clot within 10 minutes. Therefore, the mixture stayed at the top of the tube after flipping. In contrast, the blood mixed with PLGA/thrombin particles failed to form a clot even after 30 minutes (Fig. 8A).

In parallel, we monitored the strengthened network of the blood mixture via SAOS rheology. The blood mixed with PLGA/$MnO_2$/thrombin particles displayed a continuous increase of the storage modulus up to 10 Pa through 70 minutes. (Fig. 8B). The storage modulus of the resulting blood clot was twice as large as that of the blood clot formed by thrombin solution (Fig. 8C and Figure S13). In contrast, the blood mixed with PLGA/thrombin particles showed almost no increase in the storage modulus. This result indicated that PLGA/$MnO_2$/thrombin particles were able to discharge promptly and polymerize fibrinogen in the blood even with the presence of sodium citrate.

We also observed the microstructure of the blood clot formed by PLGA/$MnO_2$/thrombin particles with SEM (Fig. 8D). The images show an interconnected and highly branched fibrous network, similar to the pure fibrin gel prepared with PLGA/$MnO_2$/thrombin particles. The

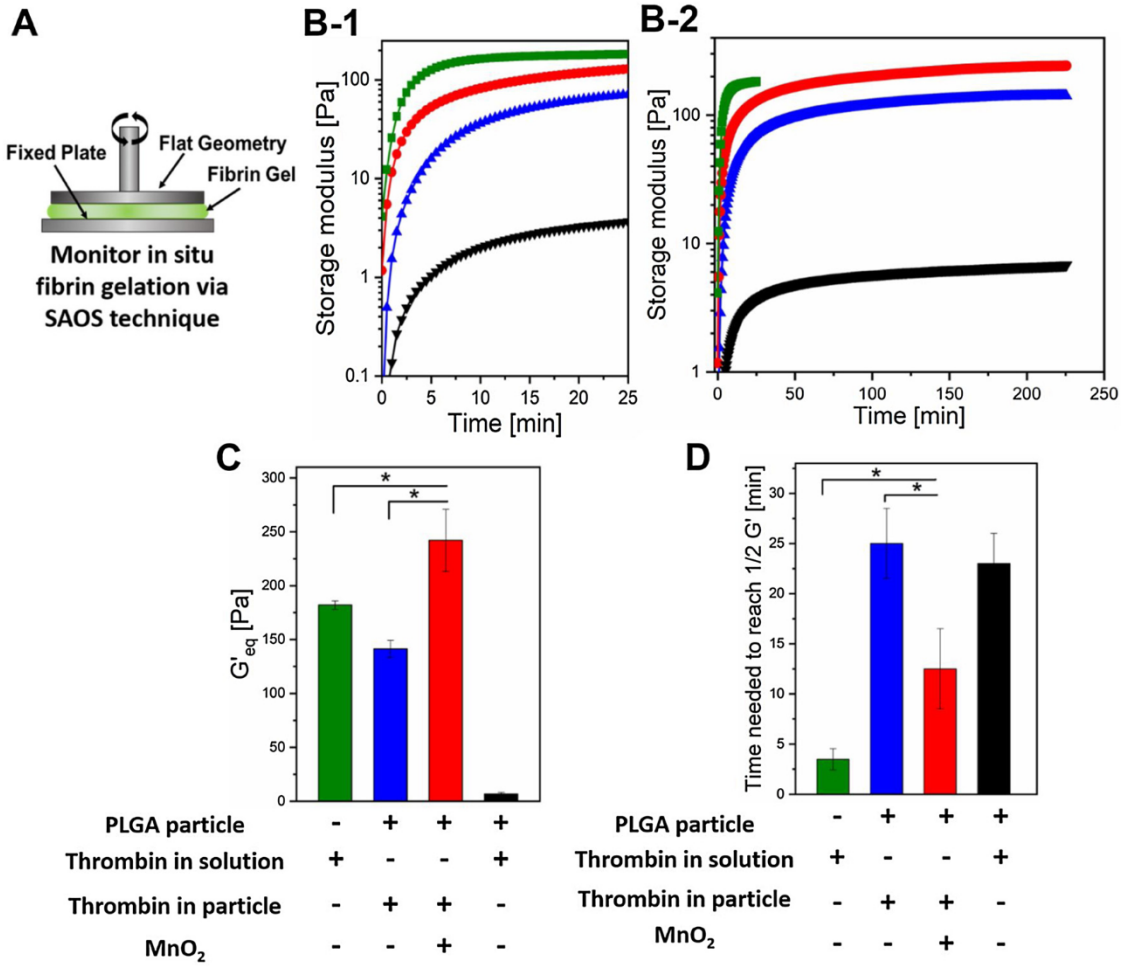


**Fig. 7.** Rheological characterization of the fibrin gel formation. (A) Schematic illustration of the experimental set-up used to monitor changes in the storage modulus of the fibrin gel. (B-1) The initial increase in the storage modulus of the fibrin gel formed by mixing the fibrinogen solution with a thrombin solution (400 ng/mL) (-■-), PLGA/$MnO_2$/thrombin particles (-●-), PLGA/thrombin particles (-▲-), or a mixture of thrombin (400 ng/mL) and blank PLGA microparticle (-▼-). The analyses were focused on the first 25 minutes and (B-2) 250 minutes. (C) Final equilibrium storage modulus (left Y-axis) and (D) time need to reach ½ of equilibrium elastic modulus of the fibrin gel formed by conditions noted on the x-axis of the plot. In (C) and (D), data points and error bars represent the average and the standard deviation of three different samples per condition, respectively. The composition of the particles used in this study was same as the condition in Fig. 4. The mass ratio between fibrinogen and particles was kept constant at 1:3.3. For all conditions, the fibrinogen concentration was kept constant at a final concentration of 12 mg/mL. * represents the statistical significance of the difference in the values between the two indicated groups (*$p < 0.05$).

**Table 1**
Gelation curve fitting parameters obtained from the gelation curves in Figure 7B-1 and B-2 using Eq. (1). $G'_{eq}$ represents the final equilibrium storage modulus, and $\beta$ is the characteristic time for gelation.

| | $G'_{sat}$ [Pa] | $\beta$ [min] | $R^2$ |
|---|---|---|---|
| **Thrombin solution** | 208.3 | 2.858 | 0.994 |
| **PLGA/$MnO_2$/thrombin particles** | 246.6 | 15.99 | 0.9379 |
| **PLGA/thrombin particles** | 149.7 | 19.6 | 0.9791 |
| **Mixture of thrombin and blank PLGA particles** | 6.96 | 16.42 | 0.9773 |

**Table 2**
Gelation curve fitting parameters obtained from the gelation curves in Figures 7B-1 and B-2 using Eq. (2). $G'_1$ is the storage modulus contributed by the branching and crosslinking reaction phase, $G'_2$ represents the storage modulus result from the second lateral growth of fibrin fibers, and $1/\tau_1$ and $1/\tau_2$ are the characteristic rate for branching and lateral growth, respectively.

| | $G'_1$ [Pa] | $1/\tau_1$ [1/min] | $G'_2$ [Pa] | $1/\tau_2$ [1/min] | $R^2$ |
|---|---|---|---|---|---|
| **Thrombin solution** | 65.35 | 0.195 | 118.4 | 0.195 | 0.9833 |
| **PLGA/$MnO_2$/thrombin particles** | 107.4 | 0.099 | 152.3 | 0.0097 | 0.9995 |
| **PLGA/thrombin particles** | 72.63 | 0.052 | 80.87 | 0.0089 | 0.9985 |
| **Mixture of thrombin and blank PLGA particles** | 4.34 | 0.052 | 3.642 | 0.005 | 0.9994 |

magnified image shown in Figure 8D-2 confirms that PLGA/$MnO_2$ particles are connected with fibrin fibers likely because the polymerization of fibrinogen occurred actively on the particle surface (yellow arrows in Fig. 8D-2).

Based on the results, we propose that our catalytic microgelator is a promising ingredient of the hemostatic agents by reproducing two major hemostasis processes: platelet-fiber association and thrombin-activated fibrin network formation [47]. Success in recapitulating the hemostasis process relies on the ability to expedite the discharge of thrombin cargos from microparticles. Otherwise, the microparticles fail to form the desired fibrin networks promptly, as demonstrated with PLGA particles loaded with thrombin only. In contrast, the catalytic microgelators exposed to $H_2O_2$ discharge thrombin actively into the blood and, in turn, promote fibrin network formation. In addition, as exhibited with SEM images and the mechanical test, PLGA/$MnO_2$/thrombin particles associated with fibrin fibers serve to stiffen the blood

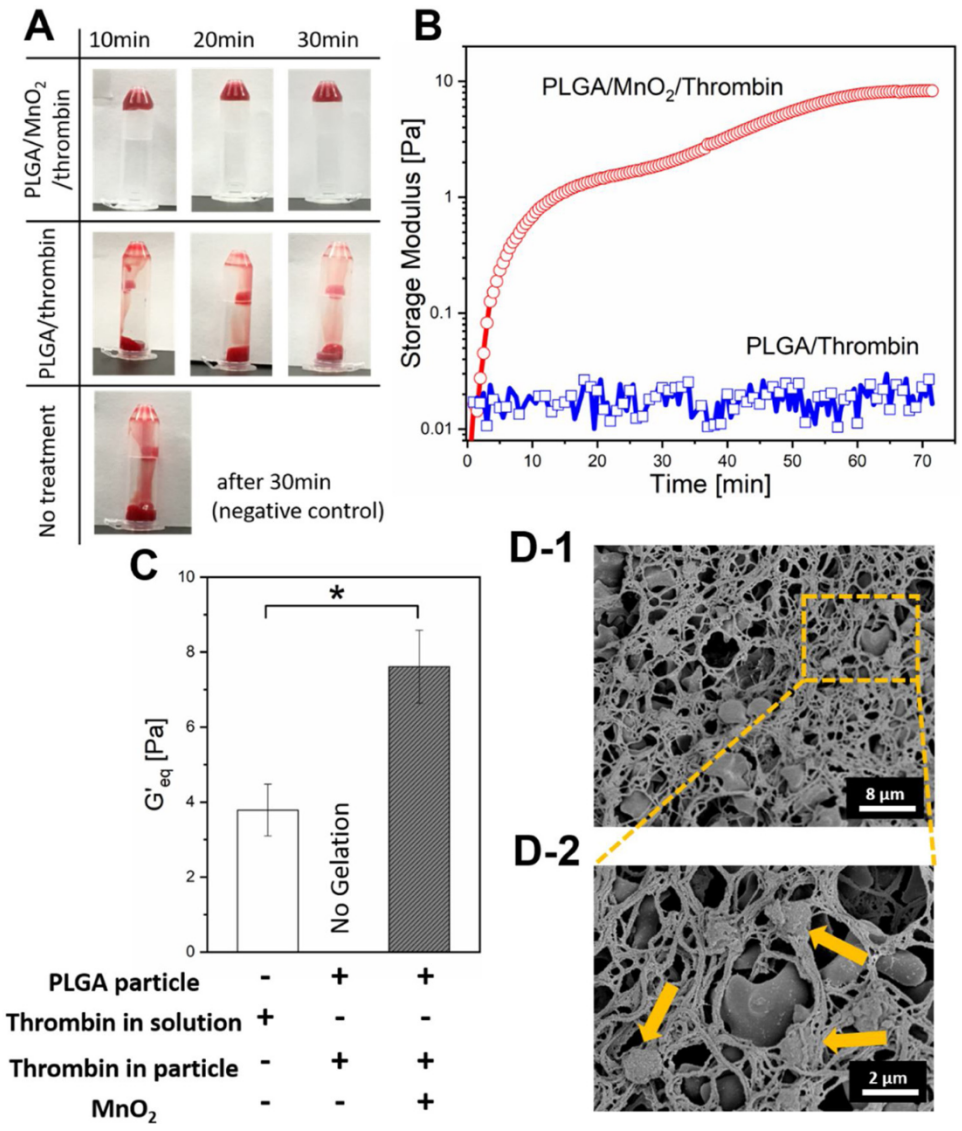


**Fig. 8.** Analysis of the blood clot formation triggered by PLGA/$MnO_2$/thrombin particles. (A) Visual characterization of the clotting of porcine blood mixed by PLGA/$MnO_2$/thrombin or PLGA/thrombin microparticles. The blood mixture was placed in the tube and flipped every ten minutes. (B) Change in the storage modulus of the blood mixed with PLGA/$MnO_2$/thrombin particles (-○-) and PLGA/thrombin particles (-□-). (C) The equilibrium storage modulus ($G'_{eq}$) of the blood mixed with thrombin solution (400 ng/mL), PLGA/$MnO_2$/thrombin particles, or PLGA/thrombin particles. (D) SEM images of a porcine blood clot formed by PLGA/$MnO_2$/thrombin particles. Yellow arrows locate the PLGA particles connected with fibrin fibers. (D-2) is a magnified view of the squared section in (D-1). Data points and error bars represent the average and standard deviation of three different samples per condition, respectively. The composition of the particles used in this study was the same as the condition in Fig. 4. The mass ratio between blood and particles was kept constant at 1:3.3. * represents the statistical significance of the difference in the values between the two indicated groups (*$p < 0.05$).

clot.

### 2.7. In Vivo Hemostatic Performance Analysis

Finally, we examined the extent to which PLGA/$MnO_2$/thrombin particles can act as a hemostatic agent by measuring time to hemostasis with a rabbit liver bleeding model (Fig. 9, details are described in the Experimental Section) [48]. Briefly, a 3 mm-diameter defect was created on the rabbit liver using a biopsy punch, and time to hemostasis was measured. The bleeding stopped after 225 seconds without any treatment. The repeated administration of PLGA/thrombin particles into the defect minimally influenced the bleeding. (Fig. 9A, Video 2). After 90 seconds, the degree of bleeding was not significantly different from the untreated condition (Fig. 9A & Video 1). Following continued administration of PLGA/thrombin particles, the bleeding stopped after 187 seconds. During this period, 50 drops of particle suspension were administered to the bleeding site. The insignificant difference of the time to hemostasis between these two groups indicated that the slow release of thrombin from the PLGA/thrombin particle is not sufficient to facilitate hemostasis. In contrast, the PLGA/$MnO_2$/thrombin particles mixed with 0.2 mM $H_2O_2$ solution at a concentration of 40 mg/ml could stop bleeding after 90 seconds (Figure 9A & B, Video 3). During this period, ten drops of particle suspension were used to control bleeding. This accelerated hemostasis is attributed to the active release of thrombin triggered by $H_2O_2$.

In the past, a series of hemostatic particles were reported to treat a severe injury that is not amenable to hemostasis. These particles were designed to reproduce the biological function of natural platelets that adhere to the bleeding site and aggregate [47,49,50,51,52,53]. For instance, liposomes were decorated with Glycoprotein Ia-IIa that adhere to the Von Willebrand factor (vWF) or collagen to promote adhesion to a bleeding site [54]. To reproduce aggregation effect of the platelets, fibrinogen or the fibrinogen-binding peptide molecules have been incorporated into the surface of microparticles [50]. However, bleeding often washes out coagulation factors, including thrombin, thus limiting fibrin network formation. In this regard, the design principle of the catalytic microgelator would be broadly useful for improving the quality of current hemostatic particles by promoting particle-fiber connection and reinforcing blood clots.

## 3. Conclusion

The results of this study demonstrate that the catalytic microgelator made of PLGA particles, $MnO_2$ nanosheets, and thrombin cargos is advantageous to extending gelation time and increasing mechanical strength of fibrin gels and blood clots. PLGA/$MnO_2$/thrombin particles suspended in media or blood containing 0.2 mM $H_2O_2$ took up and decomposed $H_2O_2$, generated $O_2$ gas, increased internal pressure, and

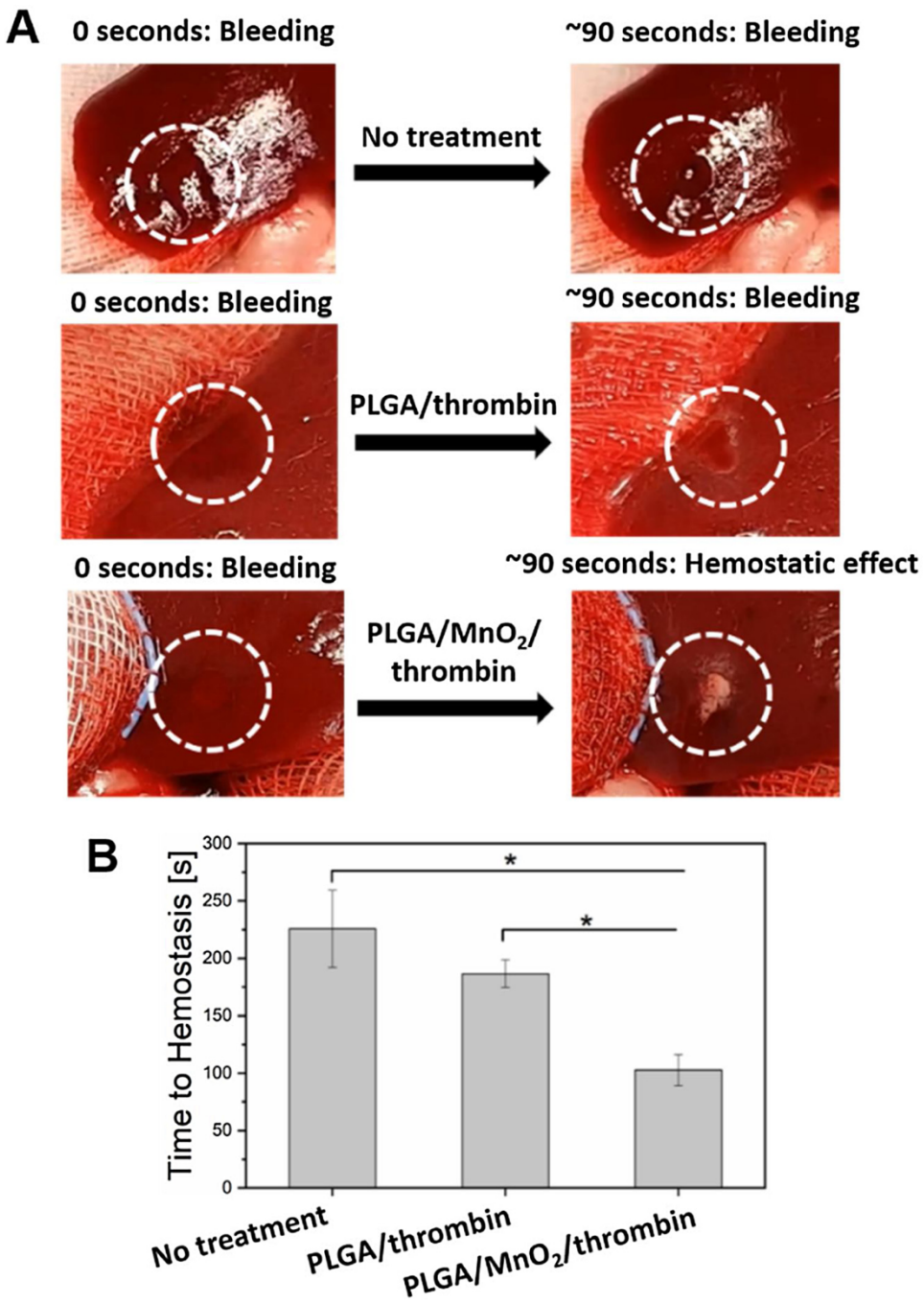


**Fig. 9.** The hemostatic capability of the PLGA/$MnO_2$/thrombin and PLGA/thrombin particles. (A) Photo images for the hemostatic effect within 90 seconds: control group without treatment (top), defect treated with PLGA/thrombin particles (middle), and defect treated with PLGA/$MnO_2$/thrombin particles (bottom). (B) Time to hemostasis in a bleeding rabbit liver treated with PLGA/$MnO_2$/thrombin and PLGA/thrombin particles. Data points and error bars represent the average and standard deviation of three different samples per condition, respectively. The particle concentration used in this study was the same as the condition in the in vitro bleeding control study. * represents the statistical significance of the difference in the values between the two indicated groups (*$p < 0.05$).

finally ejected thrombin cargos much faster than PLGA/thrombin microparticles. The fibrinogen solution or blood mixed with PLGA/$MnO_2$/thrombin particles displayed the extended gelation time by one order of magnitude. Also, the mixture formed a more rigid and elastic fibrin network or blood clots than the gel formed by mixing thrombin and fibrinogen solution. These results are attributed to the PLGA/$MnO_2$/thrombin particles that serve to sustain the presence of thrombin molecules in the fibrinogen solution or blood. It is also likely that thrombin released from PLGA/$MnO_2$ particles promotes polymerization of fibrinogen on the particle surface and, in turn, increases the number of linkages between fibrin fibers and particles. As a consequence, PLGA/$MnO_2$ particles also act as reinforcing fillers. We propose that the results of this study provide a new paradigm in controlling gelation kinetics of pre-gel solution and mechanics of the post-fibrin gel in a sophisticated manner.

## 4. Experimental Section

### 4.1. Materials

Poly(lactic-co-glycolic acid) (PLGA) with an acid end group and molecular weights ranging from 6,000 to 10,000 g/mol (lactic acid: glycolic acid = 50:50) was purchased from LACTEL Absorbable Polymers, DURECT (U.S.A). Alginate (MW ≈ 250000 g $mol^{-1)}$ was obtained from FMC Biopolymer. Cellulose filter was purchased from Millipore Inc. 2-(N-morpholino)ethanesulfonic acid (MES), potassium permanganate ($KMnO_4$), bovine serum albumin (BSA), poly(vinyl alcohol) (PVA, MW = 9000 − 10000), 1-hydroxybenzotriazole hydrate, fluorescein isothiocyanate-dextran (FITC-dextran), neocuproine (> 98%), thrombin from human plasma, fibrinogen from human plasma, and fluorescein isothiocyanate-dextran (FITC-dextran) were

purchased from Sigma-Aldrich. $H_2O_2$ (30% solution) was purchased from Macron Fine Chemicals. 1-ethyl-3- (dimethylaminopropyl)carbodiimide hydrochloride, Pierce Quantitative Peroxide Assay Kit, dichloromethane (DCM), lissamine rhodamine B ethylenediamine, copper sulfate ($CuSO_4$, > 98.6%), and fibrinogen from human plasma Alexa Fluor™ 488 conjugate were purchased from Thermo Scientific. XTT cell proliferation assay kit was purchased from Trevigen. Human thrombin ELISA kit was purchased from Innovative Research. Phosphate buffer saline was purchased from Corning. Ethanol (100%) was purchased from Decon Laboratories.

### 4.2. Synthesis of Fluorescently Labeled Alginate and Water-Dispersible $MnO_2$ nanosheets

Alginate (0.5 mmol uronic acids) dissolved in MES buffer was labeled with lissamine rhodamine B ethylenediamine using aqueous carbodiimide chemistry. 1-Hydroxybenzotriazole hydrate (0.08 mmol), lissamine rhodamine B ethylenediamine (0.0008 mmol), and 1-ethyl-3-(dimethylaminopropyl)carbodiimide hydrochloride (0.16 mmol) were added sequentially to the alginate solution. The reaction mixture was stirred at room temperature and protected from light for 4 hours. Then, the fluorescently labeled alginate was purified by dialysis against DI water over 2 days and finally lyophilized. Filtered alginate was prepared by dissolving alginate in 0.2 M MES buffer (pH 6) at a concentration of 1.0% (w/v). Then, the alginate solution was filtered with 0.22 μm cellulose filter and freeze-dried. The water-dispersible $MnO_2$ nanosheets were prepared by mixing 2.0% (w/v) alginate solution prepared with 0.2 M MES buffer with 50 mM $KMnO_4$ at 1:1 ratio. The mixture was sonicated for 30 min.

### 4.3. Assembly of PLGA Particles Loaded with Human Thrombin and $MnO_2$ Nanosheets (PLGA/$MnO_2$/thrombin particles)

PLGA/$MnO_2$/thrombin particles were prepared via double emulsification ($W_1/O/W_2$). Water phase 1 ($W_1$) was prepared by adding 50 μL thrombin (100 NIHU/mL) to a 150 μL suspension of $MnO_2$ nanosheets. The organic phase was prepared by dissolving 10 mg of PLGA in 0.75 mL of dichloromethane (DCM). Vortex mixing was conducted to form the W/O emulsion. This primary emulsion was then transferred to 6 ml of 1% (w/v) PVA solution ($W_2$). Then, the mixture was vortexed again to prepare the secondary emulsion ($W_1/O/W_2$). The mixture was continuously stirred for 4 hr to evaporate DCM. The resulting particles were washed three times and collected by centrifugation at 2,000 rpm for 10 min. In parallel, PLGA particles loading thrombin were assembled by following the same procedure in the absence of $MnO_2$ nanosheets.

### 4.4. Characterization of PLGA/$MnO_2$/thrombin particles

The optical and confocal microscopic images of PLGA particles were obtained by the optical microscope (Leica DMIL) and confocal microscope (LSM 700, Zeiss), respectively. For scanning electron microscopy (SEM) imaging of particles, PLGA particle suspensions were frozen at −20 °C and then lyophilized. The SEM images of PLGA microparticles were obtained with the HITACHI S-4700 microscope operating at 5.0 kV. The elemental analysis of manganese within PLGA particles was conducted with the inductively coupled plasma atomic emission spectroscopy (ICP/AES). The size distribution of particles was obtained by image analysis using the ImageJ software (NIH Image).

Molecular interactions between the PLGA, $MnO_2$ nanosheets, and thrombin were investigated using vibrational spectroscopy. Samples (~3 mg) were pressed onto the diamond internal reflection element (IRE) of an attenuated total reflectance infrared spectrometer (ATR-IR; Bruker, Alpha). Spectra were recorded at ambient conditions (64 scans, 2 $cm^{-1}$ resolution) with a clean diamond IRE as the background.

### 4.5. Characterization of Reactivity of PLGA/$MnO_2$/thrombin particles

Initial $H_2O_2$ decomposition rates were measured using a batch reactor with a volume of 20 cm [3]. $H_2O_2$ was added to PBS and heated to the desired temperature (300 – 320 K) while stirring the mixture at 800 rpm. $H_2O_2$ decomposition was initiated by adding PLGA/$MnO_2$ particles or $MnO_2$ nanosheets. Small aliquots (~0.5 mL) were extracted through a 0.22 μm syringe filter as a function of time. These aliquots were immediately titrated with an aqueous solution of $CuSO_4$ (8.3 mM), neocuproine (12 mM), and ethanol (25% v/v) [30]. The concentration of $H_2O_2$ in each aliquot was quantified with the absorbance at 454 nm using a visible-light spectrophotometer (Spectronic, 20 Genesys). The absorbance was back-calculated to the concentration of $H_2O_2$ using a standard curve made with solutions of known $H_2O_2$ concentration.

The long-term $H_2O_2$ decomposition over 7 hours was analyzed by adding 10 mg of PLGA particles into PBS with 0.2 mM $H_2O_2$ and incubating them at 37 °C. The mixture was shaken at 100 rpm. At different time points (1, 3, and 7 hours), the supernatant was collected by centrifuging PLGA particles. The $H_2O_2$ concentration was quantified using the Pierce Quantitative Peroxide Assay Kit.

### 4.6. Characterization of Thrombin Release from Particles

The mass of thrombin released from PLGA/$MnO_2$/thrombin or PLGA/thrombin particles was measured by suspending 10 mg of particles in 1 mL of PBS mixed with 0.2 mM $H_2O_2$ and incubating them at 37 °C. The mixture was shaken at 100 rpm. At different time points (1, 3, 7, and 20 hours), the supernatant was collected by centrifuging PLGA particles. The thrombin concentration was determined using a thrombin ELISA kit.

### 4.7. Microstructure and Bioadhesion Analysis of Fibrin Gel

The microstructure of the fibrin gel was analyzed by imaging the fibrous structure using a scanning electron microscope (HITACHI, S-4700). Fibrin gels were prepared by mixing 500 μL fibrinogen(2.5 mg/ml)/$H_2O_2$ (0.2 mM) solution with 5 mg PLGA/$MnO_2$/thrombin or PLGA/thrombin particles. Control fibrin gels were prepared by mixing thrombin and fibrinogen solutions. The thrombin concentration was adjusted to be same across conditions. After gelation overnight, the resulting fibrin gels were washed three times (5 min per wash) in DI water. Then the fibrin gels were dehydrated with an increasing percentage of ethanol. In particular, the gel samples were immersed in 30, 50, and 70% of ethanol sequentially for 1 hr. The fibrin gels were transferred to 100% ethanol and dehydrated overnight. After dehydration, the fibrin gels were dried with $CO_2$ using a critical point dryer (Tousimis). SEM images of the gels coated with Pt were taken using the HITACHI S-4700 microscope operating at 5.0 kV.

The bioadhesion of the fibrin gel was analyzed by visualizing the gel-skin interface using a scanning electron microscope (FEI, Quanta FEG 450 ESEM). Fibrin gels were prepared by mixing fibrinogen with thrombin solution, PLGA/$MnO_2$/thrombin particles, or PLGA/thrombin particles using the concentration mentioned in the microstructure study. The gel was placed in the wound-mimicking hole punched on the porcine skin explant. After gelation for 1 hr, the resulting fibrin gel was dehydrated with an increasing percentage of ethanol. In particular, the gel samples were immersed in 30, 50, and 70% of ethanol sequentially for 1 hr. The fibrin gels were transferred to 100% ethanol and dehydrated overnight. After dehydration, the fibrin gels were dried with $CO_2$ using a critical point dryer (Tousimis). SEM images of the gel-skin interface coated with Pt were taken using the FEI Quanta FEG 450 ESEM operating at 10.0 kV.

The water contact angle was measured using a contact angle goniometer (Rame-Hart). After leveling the instrument, 5 μL of deionized water droplet was placed on gel surface. The images of the droplets on the various surfaces were taken and the instrument software was used

to quantify the contact angle. Fresh samples were used for each replicate measurement.

### 4.8. In situ Confocal Imaging of Fibrin Gel Formation

The fibrous networks evolved during the gelation were imaged using a confocal microscope (LSM 700, Zeiss). The pre-gel solution consisting of fluorescently labeled fibrinogen (2.5 mg/mL) and $H_2O_2$ (0.2 mM) was mixed with rhodamine-labeled PLGA or PLGA/$MnO_2$ particles. In this study, fibrinogen was labeled with Alexa-488, while alginate coupled with $MnO_2$ nanosheets was labeled with rhodamine. PLGA particles free of $MnO_2$ nanosheets were labeled by loading rhodamine-labeled alginate via double-emulsification. The pre-gelled mixture was immediately transferred to a microscope slide with a 0.26 mm spacer and capped with a cover slide. The fibrin gel formation was monitored every 10 min for 1 hour by imaging green-colored fibrin fibers that developed over time.

### 4.9. Analysis of the Biomolecular Diffusion in the Fibrin Gel

The diffusion coefficient of dextran probes within the fibrin gel was measured using the FRAP assay. The pre-gelled mixture that contains fibrinogen (2.5 mg/mL), $H_2O_2$ (0.2 mM) and PLGA particles were mixed with 2 mg/mL fluorescein-conjugated dextran. Then, the solution was transferred to the microscope slide with a 0.26 mm spacer and capped with a cover slide. After gelation, the FRAP assay was performed using a multi-photon confocal microscope equipped with a FRAP module (LSM 710, Zeiss). A circle spot with a diameter of 0.2 mm was photobleached using a 488 nm argon laser. After photobleaching, the fluorescent image and intensity were recorded every 1 s for 150 sec. The fluorescence intensity ($F$) over time ($t$) was plotted and fitted using the Eq. (5)

$$F = A_1 + A_2 \exp(-[2T/t]) \quad (5)$$

Where $A_1$ is the initial fluorescence intensity, $A_2$ is the modified Bessel function, and $T$ is the recovery time constant. The diffusion coefficient ($D$) was then calculated using the Eq. (6)

$$D = R^2/4T \quad (6)$$

where $R$ is the radius of the photobleached spot.

### 4.10. Rheological Characterization of Gelation Kinetics and Mechanical Property of Fibrin Gel

The gelation process was monitored with small amplitude oscillatory shear rheology using an MCR702 rheometer (Anton Parr) with a parallel plate configuration (25 mm). Reaction mixtures comprised of fibrinogen (12 mg/mL) and $H_2O_2$ (0.2 mM) were mixed in a centrifuge tube with a total volume of 0.5 mL. After the addition of PLGA/$MnO_2$/thrombin particles (20 mg) or PLGA/thrombin particles (20 mg), the reaction components were thoroughly mixed with a pipette tip. Then, the mixture was quickly transferred from the tube to the rheometer bottom plate. Measurements of the storage and loss moduli were taken at 0.1 Hz under an imposed strain amplitude of 1 %. Data points were recorded every 30 seconds, and the gelation process was monitored until the moduli reached a plateau. The temperature was maintained at 37 °C using a Peltier heat exchanger. The control fibrin gel was prepared by mixing fibrinogen and thrombin solution. The thrombin concentration was kept the same as the amount of thrombin released from the PLGA/$MnO_2$/thrombin particles over 7 hours.

### 4.11. In vitro angiogenesis assay

HUVECs were suspended in the fibrinogen solution (2.5 mg/mL) containing $H_2O_2$ (0.2 mM) at a concentration of $4 \times 10^6$ cells/mL. PLGA/$MnO_2$/thrombin fibrin gel was prepared by mixing cell suspension with PLGA/$MnO_2$/thrombin particles. Then, the pre-gel solution was immediately introduced to the center HUVEC channel. The mass ratio between fibrinogen and particles was kept constant at 1:4. The control fibrin gel was prepared by mixing cell suspension with thrombin. The thrombin concentration was kept the same as the amount of thrombin released from the PLGA/$MnO_2$/thrombin particles over 7 hours. The cell suspension-gel constructs were allowed to gel for 5 min at room temperature. To fill the outer channel, the inlet reservoirs of the cell culture media channels were loaded with EGM-2 supplemented with 3 ng/mL of VEGF. The vacuum was then applied at the outlet reservoirs. Following the loading of all four reservoirs, the microfluidic platforms were incubated at 37 °C and 5% $CO_2$. The cell culture medium was removed and refilled with fresh EGM-2 culture medium every 24 h. After 3 days, cells were washed once with PBS and fixed in methanol-acetone solution (1:1 ratio) for 20 min at -20 °C. After blocking with 3% BSA in PBS for 1 h, samples were incubated overnight at 4°C with CD31 primary antibodies directly conjugated with a fluorescent marker (1:20). The cell nuclei were stained with DAPI (1:50) for 20 min at room temperature. The chips were washed three times and stored in PBS before imaging.

### 4.12. Rheological Characterization and Microstructure Analysis of Blood Clots

PLGA/$MnO_2$/thrombin particles (40 mg) or PLGA/thrombin particles (40 mg) were lyophilized and mixed with $H_2O_2$ (0.2 mM) before adding them into 1 mL of porcine blood. Blood was mixed with 3.2% citrate to prevent coagulation. The process of blood clotting was monitored by conducting SAOS rheology. After mixing of blood with particles of interests, 0.5 mL of the mixture was transferred to the bottom plate of the MCR 702 rheometer. For the control group, the pre-gel solution was prepared by mixing 1 mL of porcine blood with an equal amount of thrombin that was released by PLGA/$MnO_2$/thrombin particles over 7 hours.

To visualize the resulting blood clots, the sample mixtures mentioned above were pipetted into a centrifuge tube and flipped every 10 minutes. Scanning electron microscope (Hitachi, S-4800) was used to visualize the microstructure of the fully clotted blood clots formed by PLGA/$MnO_2$/thrombin particles. The sample was prepared in a cylindrical polydimethylsiloxane (PDMS) mold. After one hour, each sample was rinsed with PBS and fixed in the Karnovsky fixative overnight at 4 °C. Then, the fibrin clots were rinsed with PBS and fixed with 1% osmium tetraoxide for an hour. The clots were rinsed in distilled water and dehydrated by increasing concentration of ethanol gradually. The resulting clots were immersed in 30, 50, and 70% of ethanol sequentially for 1 hr per ethanol concentration. Then, the clot was transferred to 100% ethanol and dehydrated overnight. The dehydrated gel was dried with $CO_2$ using a critical point dryer (Tousimis). SEM images of the clots coated with Pt were taken with HITACHI S-4800 microscope operating at 2.0 kV.

### 4.13. In Vivo Hemostatic Performance Analysis

To examine the in vivo hemostatic ability of the PLGA/$MnO_2$/thrombin and PLGA/thrombin particles, a rabbit (healthy male New Zealand white rabbit, 3.2-3.5 kg) hemorrhaging liver model was used (n = 3 per group). Animal care and experimental procedures were conducted in accordance with the guidelines approved by the Institutional Animal Care and Use Committee (IACUC) at Yonsei University Health System, Seoul, Korea (IACUC approval No. 2017-0351). Briefly, 5 mg/kg of xylazine and 15 mg/kg of Zoletil® was intramuscularly injected every 15 min as premedication. After intubation with a 3.0 or 3.5 mm endotracheal tube, 2.0% isoflurane was used to maintain inhalation anesthesia. All the animals received crystalloid solution (10 mL/kg/h) throughout the surgical procedure. After abdominal incision, the bleeding was induced using a biopsy punch

(Integra Miltex) to create a 3 mm (diameter) defect. As a negative control, time to hemostasis was measured without any treatment. PLGA/$MnO_2$/thrombin particles or PLGA/thrombin particles were lyophilized and mixed with $H_2O_2$ (0.2 mM) before applying on the bleeding site. 0.25 ml of particle solution at a concentration of 40 mg/ml were treated in each defect site. The time to hemostasis was measured with and without treatment of the particle solution.

### 4.14. Analysis of the Toxicity of Thrombin Carriers

Mouse endothelial cell line, C166 (ATCC CRL2581), was maintained in Dulbecco's Modified Eagle Medium (DMEM) growth media supplemented with 10% FBS, 1 mM sodium pyruvate, 100 U/mL penicillin and 100 mg/mL streptomycin, and cultured at 37 °C, under an atmosphere of 5% $CO_2$ and 95% humidified air. C166 cells were seeded onto 96-well plates at a density of 5000 cells per well one day before treatment. For a certain experiment, the cell culture media was mixed with $H_2O_2$ to make the $H_2O_2$ concentration being 0.2 mM. Different concentrations of PLGA or PLGA/$MnO_2$ particles were prepared by serial dilutions in the cell culture media. The cells were then incubated with particles. 0.1 mL of PLGA or PLGA/$MnO_2$ particle suspension was added to each well. After 24 hr, 0.1 mL of growth media and 0.05 mL of XTT cell proliferation assay kit working solution were then added to each well. The cells were incubated for 3 h at 37 °C. The absorbance values of the solution at a wavelength of 490 and 630 nm were measured by using the microplate spectrophotometer (TECAN, Infinite 200 Pro). The relative metabolic activity of cells was quantified as [($A_{490}$/$A_{630}$) of each group / ($A_{490}$/$A_{630}$) of control group] where $A_{490}$ and $A_{630}$ represent absorbance at 490 nm and 630 nm respectively. The control group represents the group in which only media was added to each well.

## 5. Statistical Analysis

Three samples were analyzed per condition, and the data were presented as mean ± standard deviation unless otherwise specified. To determine significance, comparisons between groups were performed by one-way ANOVA followed by Tukey's post hoc analyses. Data were considered significant for p values less than 0.05.

## 6. Supporting Information

The Supporting Information is available free of charge.

Water-dispersible $MnO_2$ nanosheets complexed with alginate, SEM images of PLGA particles, FTIR spectra of PLGA particle, cumulative $O_2$ generated through the $H_2O_2$ decomposition, $H_2O_2$ decomposition curve under different conditions, theoretical calculation of the difference between internal pressure and external pressure of PLGA/$MnO_2$ particles, quantitative analysis of fluorescent-labeled $MnO_2$ intensity change over time, evaluation of the bioadhesion of fibrin gel, evaluation of surface water contact angle of fibrin gel, gelation curve fitting, in vitro angiogenesis assay, blood clot formation triggered by thrombin (PDF)

## Author Contributions

Y.-T.H. and H.K. conceived the idea including designing the experiments. Y.-T.H., D.T.B., and D.W.F. performed the H2O2 decomposition experiment and analysis. Y.H., C.-W.L., and S.A.R. performed rheological measurements and analysis. D.-H.K, Y.J.L., and H.-J.S. assisted with the in vivo bleeding control experiment. Y.-T.H. performed the angiogenesis experiment, and H.J assisted with the microfluidics design. L.G.S assisted with porcine blood acquisition. Y.-T.H, and Y.S developed the fabrication process. Y.-T.H. wrote the manuscript with input from all authors.

The authors declare no competing financial interest.

## Acknowledgments

We appreciate the financial support from the National Institutes of Health (1 R21 HL131469) and the National Science Foundation (STC-EBICS Grant CBET-0939511, and CBET-15531377). Electron microscopy was performed at the Frederick Seitz Materials Research Laboratory Central Facilities at the University of Illinois. ICP was conducted at Microanalysis Laboratory (SCS CORES) at the University of Illinois. The authors acknowledge Anton Paar for their academic V.I.P program to S.A.R. Y.-T.H thanks J.Soh. for the graphic assists. Y.-T.H thanks J.Leong. and J.Y.Teo for scientific discussions.

## Appendix A. Supplementary data

Supplementary material related to this article can be found, in the online version, at doi:https://doi.org/10.1016/j.jconrel.2019.10.029.

## References

[1] A. Henschen, J. Mcdonagh, R.F.A. Zwaal, H.C. Hemker (Eds.), Blood Coagulation, vol. 13, Elsevier, 1986, pp. 171–241.
[2] J.W. Weisel, The Mechanical Properties of Fibrin for Basic Scientists and Clinicians, Biophys. Chem. 112 (2004) 267–276.
[3] E.A. Ryan, L.F. Mockros, J.W. Weisel, L. Lorand, Structural Origins of Fibrin Clot Rheology, Biophys J 77 (1999) 2813–2826.
[4] J.W. Weisel, Structure of Fibrin: Impact on Clot Stability, J. Thromb. Haemost. 5 (Suppl 1) (2007) 116–124.
[5] B. Blombäck, B. Hessel, D. Hogg, L.A. Therkildsen, Two-Step Fibrinogen–Fibrin Transition in Blood Coagulation, Nature 275 (5680) (1978) 501–505 1978, 275.
[6] R.A. Clark, Fibrin and Wound Healing, Ann N Y Acad Sci 936 (2001) 355–367.
[7] N. Laurens, P. KOOLWIJK, M.P.M.D. MAAT, Fibrin Structure and Wound Healing, Journal of Thrombosis and Haemostasis 4 (2006) 932–939.
[8] T.A.E. Ahmed, E.V. Dare, M. Hincke, Fibrin: a Versatile Scaffold for Tissue Engineering Applications, Tissue Eng Part B Rev 14 (2008) 199–215.
[9] I. Catelas, N. Sese, B.M. Wu, J.C.Y. Dunn, S. Helgerson, B. Tawil, Human Mesenchymal Stem Cell Proliferation and Osteogenic Differentiation in Fibrin Gels in Vitro 12 (2006), pp. 2385–2396 https://home.liebertpub.com/ten.
[10] F.H. Silver, M.-C. Wang, G.D. Pins, Preparation and Use of Fibrin Glue in Surgery, Biomaterials 16 (1995) 891–903.
[11] J. Liu, Y. Tan, H. Zhang, Y. Zhang, P. Xu, J. Chen, Y.-C. Poh, K. Tang, N. Wang, B. Huang, Soft Fibrin Gels Promote Selection and Growth of Tumorigenic Cells, Nat Mater 11 (2012) 734–741.
[12] S.B. Patil, S.Z. Inamdar, K.R. Reddy, A.V. Raghu, S.K. Soni, R.V. Kulkarni, Novel Biocompatible Poly(Acrylamide)-Grafted-Dextran Hydrogels: Synthesis, Characterization and Biomedical Applications, Journal of Microbiological Methods 159 (2019) 200–210.
[13] K. Kolehmainen, S.M. Willerth, Preparation of 3D Fibrin Scaffolds for Stem Cell Culture Applications, J Vis Exp (2012) e3641.
[14] R. DeVolder, H.-J. Kong, Hydrogels for in Vivo-Like Three-Dimensional Cellular Studies, Wiley Interdiscip Rev Syst Biol Med 4 (2012) 351–365.
[15] N. Dubey, Neuronal Contact Guidance in Magnetically Aligned Fibrin Gels: Effect of Variation in Gel Mechano-Structural Properties, Biomaterials 22 (2001) 1065–1075.
[16] M.E. Carr, D.A. Gabriel, J. McDonagh, Influence of Ca2+ on the Structure of Reptilase-Derived and Thrombin-Derived Fibrin Gels, Biochem. J. 239 (1986) 513–516.
[17] H. Zhao, L. Ma, J. Zhou, Z. Mao, C. Gao, J. Shen, Fabrication and Physical and Biological Properties of Fibrin Gel Derived From Human Plasma, Biomed Mater 3 (2008) 015001.
[18] A.C. Brown, T.H. Barker, Fibrin-Based Biomaterials: Modulation of Macroscopic Properties Through Rational Design at the Molecular Level, Acta Biomater 10 (2014) 1502–1514.
[19] Z. Bagoly, Z. Koncz, J. Harsfalvi, L. Muszbek, Factor XIII, Clot Structure, Thrombosis, Thrombosis Research 129 (2012) 382–387.
[20] Y. Seo, J. Leong, J.Y. Teo, J.W. Mitchell, M.U. Gillette, B. Han, J. Lee, H. Kong, Active Antioxidizing Particles for on-Demand Pressure-Driven Molecular Release, ACS Appl. Mater. Interfaces 9 (2017) 35642–35650.
[21] J.Y. Teo, Y. Seo, E. Ko, J. Leong, Y.-T. Hong, Y.Y. Yang, H. Kong, Surface Tethering of Stem Cells with H2O2-Responsive Anti-Oxidizing Colloidal Particles for Protection Against Oxidation-Induced Death, Biomaterials 201 (2019) 1–15.
[22] P.A. Hyslop, Z. Zhang, D.V. Pearson, L.A. Phebus, Measurement of Striatal H2O2 by Microdialysis Following Global Forebrain Ischemia and Reperfusion in the Rat: Correlation with the Cytotoxic Potential of H2O2 in Vitro, Brain Res. 671 (1995) 181–186.
[23] N. Ojha, S. Roy, G. He, S. Biswas, M. Velayutham, S. Khanna, P. Kuppusamy, J.L. Zweier, C.K. Sen, Assessment of Wound-Site Redox Environment and the Significance of Rac2 in Cutaneous Healing, Free Radic. Biol. Med. 44 (2008) 682–691.
[24] H. Rafati, A.G.A. Coombes, J. Adler, J. Holland, S.S. Davis, Protein-Loaded Poly(Dl-Lactide-Co-Glycolide) Microparticles for Oral Administration: Formulation,

Structural and Release Characteristics, Journal of Controlled Release 43 (1997) 89–102.
[25] I.D. Rosca, F. Watari, M. Uo, Microparticle Formation and Its Mechanism in Single and Double Emulsion Solvent Evaporation, Journal of Controlled Release 99 (2004) 271–280.
[26] D.P. Suhas, H.M. Jeong, T.M. Aminabhavi, A.V. Raghu, Preparation and Characterization of Novel Polyurethanes Containing 4,4′-{Oxy-1,4-Diphenyl Bis (Nitromethylidine)}Diphenol Schiff Base Diol, Polymer Engineering & Science 54 (2014) 24–32.
[27] A.V. Raghu, G.S. Gadaginamath, H.M. Jeong, N.T. Mathew, S.B. Halligudi, T.M. Aminabhavi, Synthesis and Characterization of Novel Schiff Base Polyurethanes, Journal of Applied Polymer Science 113 (2009) 2747–2754.
[28] M.A. Hasan, M.I. Zaki, L. Pasupulety, K. Kumari, Promotion of the Hydrogen Peroxide Decomposition Activity of Manganese Oxide Catalysts, Applied Catalysis A: General 181 (1999) 171–179.
[29] S.-H. Do, B. Batchelor, H.-K. Lee, S.-H. Kong, Hydrogen Peroxide Decomposition on Manganese Oxide (Pyrolusite): Kinetics, Intermediates, and Mechanism, Chemosphere 75 (2009) 8–12.
[30] D.T. Bregante, N.E. Thornburg, J.M. Notestein, D.W. Flaherty, Consequences of Confinement for Alkene Epoxidation with Hydrogen Peroxide on Highly Dispersed Group 4 and 5 Metal Oxide Catalysts, Acs Catalysis 8 (2018) 2995–3010.
[31] W. Abdelwahed, G. Degobert, S. Stainmesse, H. Fessi, Freeze-Drying of Nanoparticles: Formulation, Process and Storage Considerations, Adv. Drug Deliv. Rev. 58 (2006) 1688–1713.
[32] N.A. Williams, G.P. Polli, The Lyophilization of Pharmaceuticals: a Literature Review, J Parenter Sci Technol 38 (1984) 48–59.
[33] J.-H. Oak, H. Cai, Attenuation of Angiotensin II Signaling Recouples eNOS and Inhibits Nonendothelial NOX Activity in Diabetic Mice, Diabetes 56 (2007) 118–126.
[34] H. Sah, R. Toddywala, Y.W. Chien, The Influence of Biodegradable Microcapsule Formulations on the Controlled Release of a Protein, Journal of Controlled Release 30 (1994) 201–211.
[35] Y. Yeo, K. Park, Control of Encapsulation Efficiency and Initial Burst in Polymeric Microparticle Systems, Arch. Pharm. Res. 27 (2004) 1–12.
[36] M. Jarzynska, M. Pietruszka, The Application of the Kedem–Katchalsky Equations to Membrane Transport of Ethyl Alcohol and Glucose, Desalination 280 (2011) 14–19.
[37] G. Suchanek, Mechanistic Equations for Membrane Transport of Multicomponent Solutions, Gen. Physiol. Biophys. 25 (2006) 53–63.
[38] R.H. Ottewill, Stability of Polymer Colloids. Polymeric Dispersions: Principles and Applications 4 Springer, Dordrecht: Dordrecht, 1997, pp. 31–48.
[39] D.M. Soumpasis, Theoretical Analysis of Fluorescence Photobleaching Recovery Experiments, Biophysical Journal 41 (1983) 95–97.
[40] F. Brandl, F. Kastner, R.M. Gschwind, T. Blunk, J. Tessmar, A. Göpferich, Hydrogel-Based Drug Delivery Systems: Comparison of Drug Diffusivity and Release Kinetics, J Control Release 142 (2010) 221–228.
[41] D.P. Suhas, T.M. Aminabhavi, H.M. Jeong, A.V. Raghu, Hydrogen Peroxide Treated Graphene as an Effective Nanosheet Filler for Separation Application, Rsc Adv 5 (2015) 100984–100995.
[42] D.P. Suhas, T.M. Aminabhavi, A.V. Raghu, Para-Toluene Sulfonic Acid Treated Clay Loaded Sodium Alginate Membranes for Enhanced Pervaporative Dehydration of Isopropanol, Applied Clay Science 101 (2014) 419–429.
[43] Merlini, P. A.; Ardissino, D. Laboratory Measurement of Thrombin Activity—What Every Clinician Scientist Needs to Know. J Thromb Thrombol 2, 85–92.
[44] G.W. Scott Blair, J. Burnett, An Equation to Describe the Rate of Setting of Blood and Milk, Biorheology 1 (1963) 183–191.
[45] M. Kaibara, Rheological Studies on Blood Coagulation and Network Formation of Fibrin, Polymer Gels and Networks 2 (1994) 1–28.
[46] V.W.M. van HINSBERGH, A. COLLEN, P. KOOLWIJK, Role of Fibrin Matrix in Angiogenesis, Annals of the New York Academy of Sciences 936 (2001) 426–437.
[47] C.L. Modery-Pawlowski, L.L. Tian, V. Pan, K.R. McCrae, S. Mitragotri, A. Gupta Sen, Approaches to Synthetic Platelet Analogs, Biomaterials 34 (2013) 526–541.
[48] F. Chen, X. Cao, X. Chen, J. Wei, C. Liu, Calcium-Modified Microporous Starch with Potent Hemostatic Efficiency and Excellent Degradability for Hemorrhage Control, J. Mater. Chem. B 3 (2015) 4017–4026.
[49] J.P. Bertram, C.A. Williams, R. Robinson, S.S. Segal, N.T. Flynn, E.B. Lavik, Intravenous Hemostat: Nanotechnology to Halt Bleeding, Sci Transl Med 1 (2009) 11ra22.
[50] M. Levi, P.W. Friederich, S. Middleton, P.G. de Groot, Y.P. Wu, R. Harris, B.J. Biemond, H.F. Heijnen, J. Levin, J.W. Cate ten, Fibrinogen-Coated Albumin Microcapsules Reduce Bleeding in Severely Thrombocytopenic Rabbits, Nat. Med. 5 (1999) 107–111.
[51] S. Takeoka, Y. Teramura, Y. Okamura, E. Tsuchida, M. Handa, Y. Ikeda, Rolling Properties of rGPIbalpha-Conjugated Phospholipid Vesicles with Different Membrane Flexibilities on vWf Surface Under Flow Conditions, Biochem. Biophys. Res. Commun. 296 (2002) 765–770.
[52] A.C. Anselmo, C.L. Modery-Pawlowski, S. Menegatti, S. Kumar, D.R. Vogus, L.L. Tian, M. Chen, T.M. Squires, A. Gupta Sen, S. Mitragotri, Platelet-Like Nanoparticles: Mimicking Shape, Flexibility, and Surface Biology of Platelets to Target Vascular Injuries, Acs Nano 8 (2014) 11243–11253.
[53] Y. Okamura, T. Fujie, H. Maruyama, M. Handa, Y. Ikeda, S. Takeoka, Prolonged Hemostatic Ability of Polyethylene Glycol-Modified Polymerized Albumin Particles Carrying Fibrinogen Gamma-Chain Dodecapeptide, Transfusion 47 (2007) 1254–1262.
[54] T. Nishiya, M. Kainoh, M. Murata, M. Handa, Y. Ikeda, Reconstitution of Adhesive Properties of Human Platelets in Liposomes Carrying Both Recombinant Glycoproteins Ia/IIa and Ib Alpha Under Flow Conditions: Specific Synergy of Receptor-Ligand Interactions, Blood 100 (2002) 136–142.